AGU PUBLICATIONS

JGR

Journal of Geophysical Research: Solid Earth

RESEARCH ARTICLE
10.1002/2016JB012984

Key Points:
- Paleomagnetism aids distinction and correlations of rheomorphic ignimbrites
- Optimal paleomagnetic field and laboratory methods are suggested

Supporting Information:
- Supporting Information S1
- Table S1
- Table S2
- Table S3
- Table S4
- Table S5
- Table S6

Correspondence to:
D. R. Finn,
dfinn@ucsc.edu

Citation:
Finn, D. R., R. S. Coe, E. Brown, M. Branney, M. Reichow, T. Knott, M. Storey, and B. Bonnichsen (2016), Distinguishing and correlating deposits from large ignimbrite eruptions using paleomagnetism: The Cougar Point Tuffs (mid-Miocene), southern Snake River Plain, Idaho, USA, *J. Geophys. Res. Solid Earth*, *121*, 6293–6314, doi:10.1002/2016JB012984.

Received 9 MAR 2016
Accepted 15 AUG 2016
Accepted article online 16 AUG 2016
Published online 17 SEP 2016

©2016. American Geophysical Union. All Rights Reserved.

Distinguishing and correlating deposits from large ignimbrite eruptions using paleomagnetism: The Cougar Point Tuffs (mid-Miocene), southern Snake River Plain, Idaho, USA

David R. Finn[1], Robert S. Coe[1], Ethan Brown[1], Michael Branney[2], Marc Reichow[2], Thomas Knott[2], Michael Storey[3], and Bill Bonnichsen[4]

[1]Earth and Planetary Science Department, University of California, Santa Cruz, California, USA, [2]Department of Geology, University of Leicester, Leicester, UK, [3]Quadlab, Natural History Museum of Denmark, University of Copenhagen, Copenhagen, Denmark, [4]Idaho Geological Survey (retired), Moscow, Idaho, USA

Abstract In this paper, we present paleomagnetic, geochemical, mineralogical, and geochronologic evidence for correlation of the mid-Miocene Cougar Point Tuff (CPT) in southwest Snake River Plain (SRP) of Idaho. The new stratigraphy presented here significantly reduces the frequency and increases the scale of known SRP ignimbrite eruptions. The CPT section exposed at the Black Rock Escarpment along the Bruneau River has been correlated eastward to the Brown's Bench escarpment (six common eruption units) and Cassia Mountains (three common eruption units) regions of southern Idaho. The CPT records an unusual pattern of geomagnetic field directions that provides the basis for robust stratigraphic correlations. Paleomagnetic characterization of eruption units based on geomagnetic field variation has a resolution on the order of a few centuries, providing a strong test of whether two deposits could have been emplaced from the same eruption or from temporally separate events. To obtain reliable paleomagnetic directions, the anisotropy of anhysteretic remanence was measured to correct for magnetic anisotropy, and an efficient new method was used to remove gyroremanence acquired during alternating field demagnetization.

1. Introduction

Migration of the Yellowstone hot spot across continental U.S. during the Miocene has left a trail of time-transgressive bimodal rhyolitic to basaltic volcanism in the Snake River Plain (SRP) of Idaho (Figure 1). Along the axis of the SRP younger basalt lavas overlie voluminous rhyolitic ignimbrites and lavas, whereas in hills flanking the SRP successions of outflow rhyolitic ignimbrites are well exposed [*Armstrong et al.*, 1975, 1980; *Bonnichsen and Citron*, 1982; *Knott et al.*, 2016a; *Manley and McIntosh*, 2002; *Morgan and McIntosh*, 2005; *Pierce and Morgan*, 1992]. The ignimbrites are intensely welded and rheomorphic outflow sheets from large, environmentally catastrophic explosive Yellowstone hot spot eruptions [*Branney et al.*, 2008]. Development of a regional ignimbrite stratigraphy (Figure 2) by correlation of individual eruption units (e.g., cooling units) is essential to constrain the eruption volumes and eruption frequencies and to better understand the causal relationship between magma productivity, tectonics, and climate change.

In this contribution, we use paleomagnetism, geochronology, and whole-rock and mineral chemistry for stratigraphic correlation of the well-recognized [e.g., *Bonnichsen and Citron*, 1982] Cougar Point Tuff (CPT) units with other eruption units exposed in the nearby Brown's Bench (Figure 3) escarpment and the Cassia Mountain regions of southern Idaho (Figure 1). Description of the local successions at the Black Rock (Cougar Point Tuffs) and Brown's Bench (Rogerson Formation) escarpments and Cassia Mountains (Cassia Formation) can be found in *Bonnichsen and Citron* [1982], *Knott et al.* [2016a], and *Knott et al.* [2016b], respectively.

Of the various techniques we have employed for identification and correlation of eruption units, paleomagnetism has proved exceptionally useful. The method proposed by *Bogue and Coe* [1981] was used to quantify the paleomagnetic correlation between individual eruptions and sequences of eruptions. There are, however, several pitfalls that can hinder determination of the primary paleomagnetic remanence direction of rheomorphic rhyolitic ignimbrites, such as in the SRP. These pitfalls include, but are not limited to, magnetic overprinting during growth or alteration of magnetic minerals at low temperatures, large magnetic anisotropy, and acquisition of gyroremanence magnetization during alternating field (AF) demagnetization.

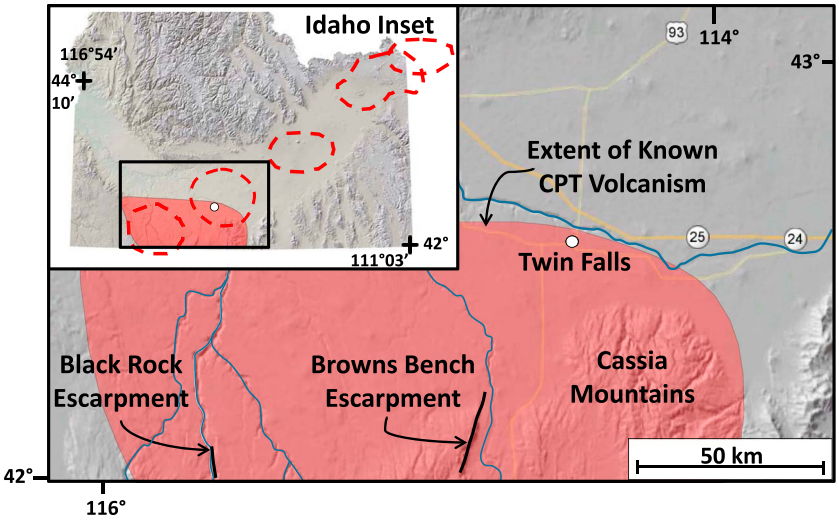

Figure 1. Map of the Snake River Plain showing the sampling locations. The inset map shows the southern two thirds of Idaho with the approximate locations of putative eruptive centers (red dashed circles) and location of the enlarged area (black rectangle) indicated. The shaded red overlay shows the currently known extent of the Cougar Point Tuff (CPT) eruptions. The Grasmere escarpment ignimbrite was included in this areal extent because it is thought to be part of the CPT, although the exact correlation to CPT units with designated roman numerals remains uncertain.

Therefore, it is important that paleomagnetic correlations are also supported by field, mineralogical, geochemical, and radioisotopic data.

1.1. Snake River-Type Ignimbrites

Pyroclastic deposits along the margins of the central Snake River Plain exemplify a newly defined class of volcanism, known as Snake River (SR)-type volcanism [*Branney et al.*, 2008]. The most impressive section of ignimbrites of this type in the Snake River Plain is the ~450 m tall Black Rock escarpment [*Bonnichsen and*

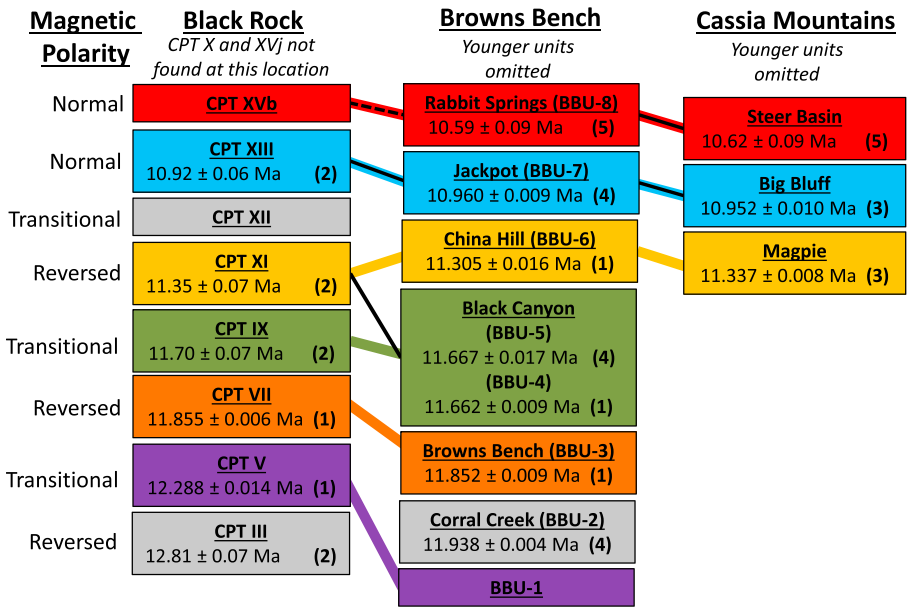

Figure 2. Correlations between the Black Rock and Brown's Bench escarpments and the Cassia Mountains in southern Idaho. The thin black connecting lines highlight the proposed correlations by *Ellis et al.* [2012]. Radioisotopic age data: (1) this study, (2) *Bonnichsen et al.* [2008], (3) *Knott et al.* [2016a], (4) *Knott et al.* [2016b], and (5) *Ellis et al.* [2012]. All argon ages have been recalculated to an age of 28.172 Ma for the Fish Canyon Tuff standard age [*Rivera et al.*, 2011]. Note that we consider remanence directions that are pointed southward and down to be transitional.

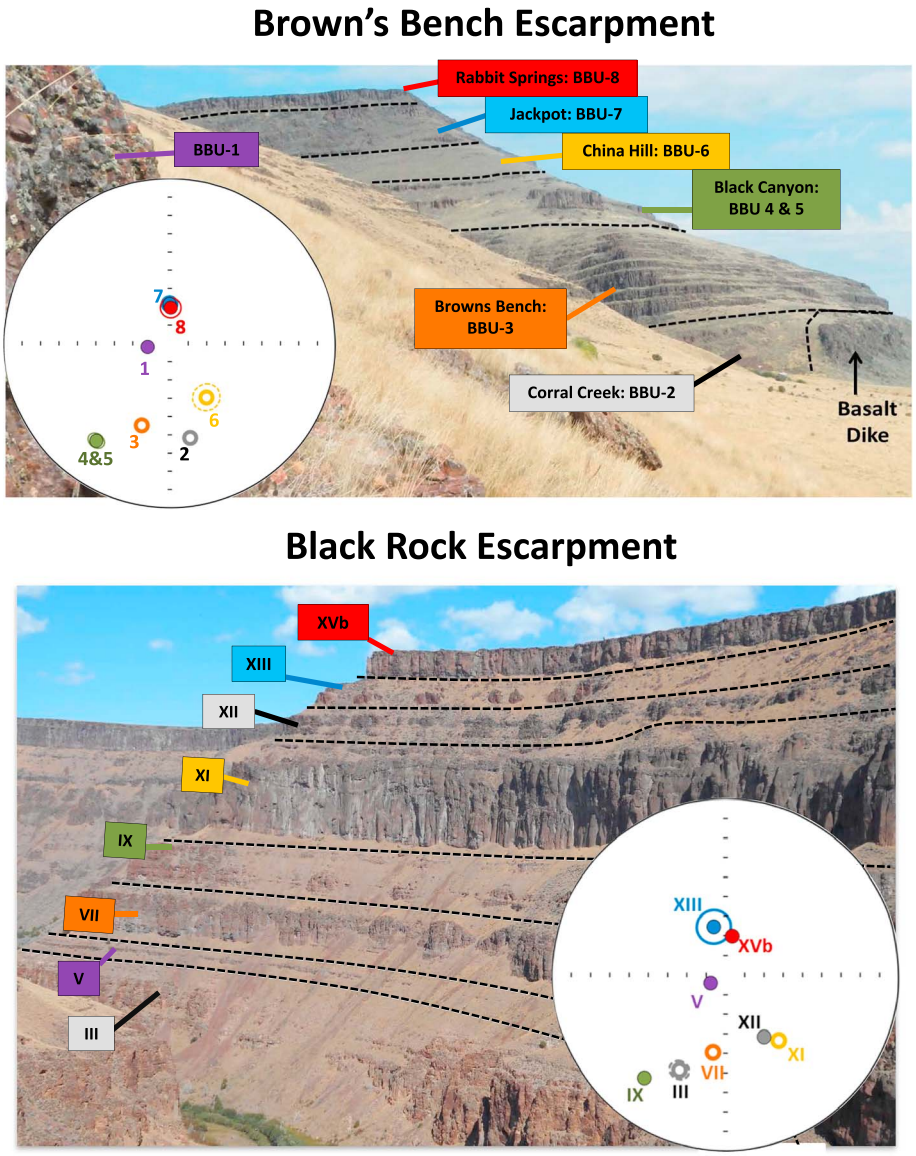

Figure 3. Photo of the Brown's Bench and Black Rock escarpment sampling locations (see Figure 1) with the units labeled and color coded based on the proposed correlations. Note that two names are given for each unit in the Brown's Bench escarpment following the new nomenclature by *Knott et al.* [2016b] and that initially proposed by *Bonnichsen et al.* [2008] (e.g., BBU-6). A stereonet projection showing site-mean directions is shown for each location. The hollow symbols are upper hemisphere.

Citron, 1982] along the Bruneau River Canyon, Idaho, with eight individual eruption units (Figures 1, 3, and 4). Many of the same CPT eruption units have been identified in the Jarbidge Canyons a little over 20 km east [*Bonnichsen and Citron*, 1982]. The Brown's Bench escarpment, ~70 km east of Black Rock escarpment (Figure 1), exposes 10 individual ignimbrite eruption units [*Knott et al.*, 2016b] but with thinner representatives of the correlative units. The Cassia Mountains, which lie ~100 km east (Figure 1), expose 10 individual ignimbrite eruption units [*Knott et al.*, 2016a], with as many as 6 in a single unfaulted stratigraphic section. Successively younger units are exposed toward the east.

SR-type ignimbrites are characteristically large-volume, rhyolitic, metaluminous and ferroan, emplaced at high temperature, and have low $\delta^{18}O$ [*Bindeman and Simakin*, 2014; *Branney et al.*, 2008]. They are intensely welded and devitrified, strongly rheomorphic, lack obvious glass shards and vitroclastic textures, and have upper autobreccias and associated laminated ashfall layers. Several SR-type ignimbrites are of a lithology that resembles massive or flow-laminated rhyolitic lavas [*Branney and Kokelaar*, 1992] and are primarily

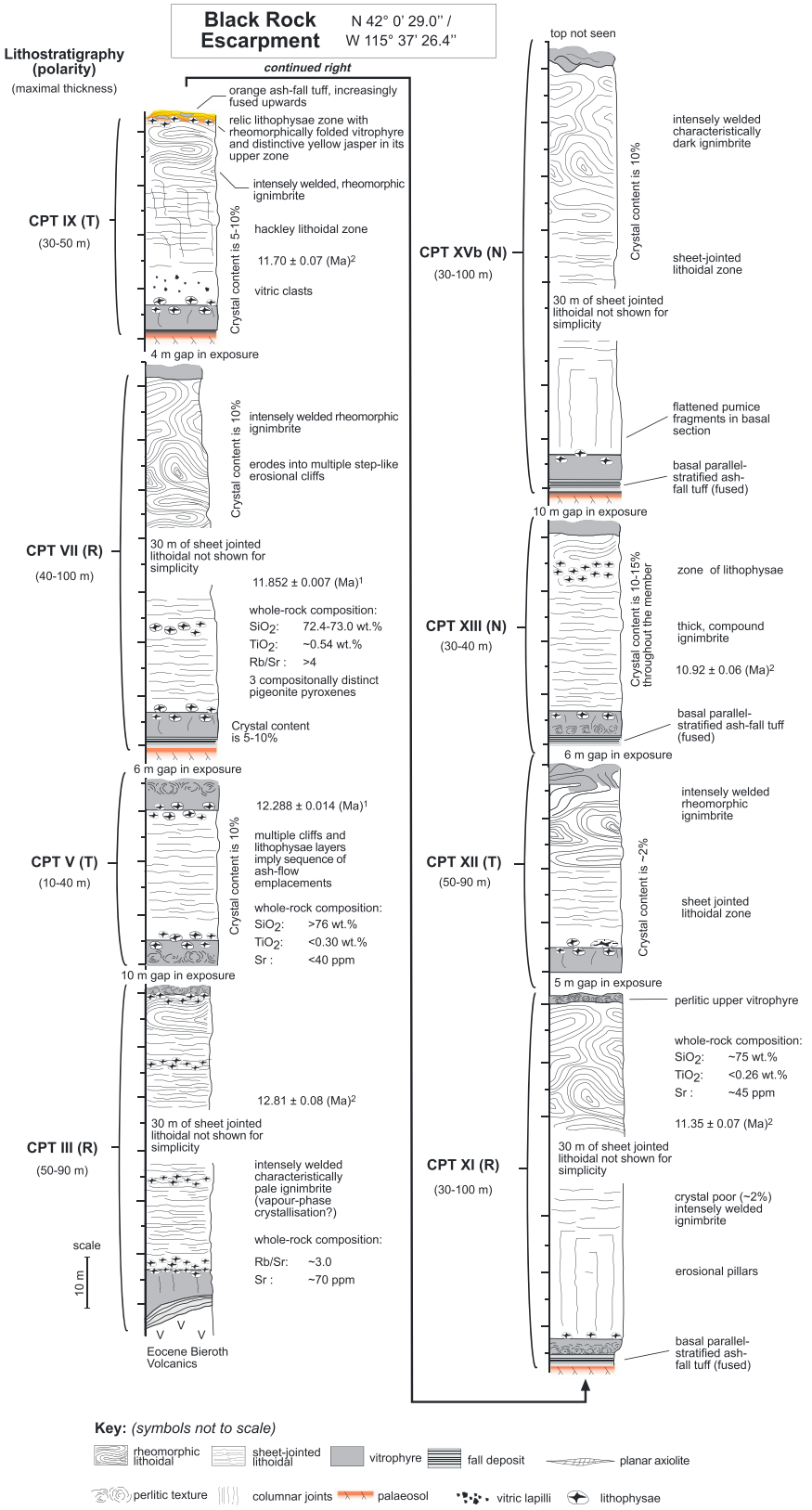

Figure 4. Generalized vertical stratigraphy of the Cougar Point Tuff formation showing the physical features of each of the eight members at the Black Rock escarpment in southern Idaho. Argon ages: (1) this study and (2) Bonnichsen *et al.* [2008]; all recalculated to *Rivera et al.* [2011].

distinguishable in the field from lavas by their thinly tapering distal margins and the absence of significant basal autobreccia. Most SR-type ignimbrites have a thick central crystallized (lithoidal) zone and thinner upper and lower glassy (vitrophyre) marginal zones. The central lithoidal zones typically pinch out distally toward the distal ignimbrite margins, where the deposit is thin and so chilled rapidly.

Finn et al. [2015] presented hysteresis, temperature susceptibility, low-field-induced magnetic anisotropy, thermal remanence anisotropy, and magnetic remanence measurements on a set of samples collected in a vertical profile through a typical SR-type ignimbrite (the Grey's Landing ignimbrite). From their results and a review of the literature, *Finn et al.* [2015] concluded that the magnetic remanence of SR-type strongly welded ignimbrites was carried by large magmatic titanium-rich magnetite grains, postmagmatic small titanium-poor magnetite grains, and minor amounts of secondary titanohematite grains. The magnetic remanence and remanence anisotropy are dominantly carried by the titanium-poor magnetite grains, which nucleated in the volcanic glass at high temperatures after and possibly during emplacement [*Finn et al.*, 2015; *Geissman et al.*, 1983; *Pioli et al.*, 2008; *Wolff et al.*, 1989]. These observations suggest that the preferential nucleation of fine-grained magnetite along the margins of highly strained glass shards caused the magnetic fabric to inherit the preexisting strain fabric in the glass, a process largely dependent on cooling time. Many magnetic properties, including anisotropy, susceptibility, coercivity, dominant unblocking temperature, and remanence direction and strength vary from the quickly chilled ignimbrite base to the more slowly cooled interior [*Finn et al.*, 2015; *Pioli et al.*, 2008; *Schlinger et al.*, 1988]. Chemical alteration of magnetic minerals during and possibly shortly after initial cooling may also have contributed to acquisition of remanence subparallel to the paleofield direction. In contrast, alteration and growth of new minerals long after emplacement will produce a detectable magnetic overprint in a different paleofield direction.

2. Paleomagnetism

2.1. Paleomagnetic Methods

Paleomagnetic cores were collected with a gasoline-powered hand drill and oriented with a magnetic compass. Correction for the local magnetic field anomaly was made individually for each core using the observed azimuth of the Sun. The central rheomorphic folded zone and devitrified interior was the preferred choice for collection of paleomagnetic samples. Stratigraphic sections containing multiple cooling units were sampled at the Black Rock and Brown's Bench escarpments and Cassia Mountains. At the Black Rock escarpment sampling the entire stratigraphic succession entitled collecting from two locations that were less than 1 km apart (see Figures S1 and S2 in the supporting information), but strata in the intervening exposed ground are nonfaulted and lack any detectable changes in dip. Paleomagnetic sites from CPT III, V, VII, and IX were collected at the western section (southern Black Rock escarpment), and those from CPT VII, IX, XII, XIII, and XVb were from the eastern section, which is a tributary drainage known as Hole in the Ground, used to access the Bruneau Canyon at the southern end of the Black Rock escarpment.

Laboratory work was conducted at the University of California, Santa Cruz. Magnetic remanence was primarily removed with alternating field (AF) rather than thermal demagnetization. Magnetic remanence measurement, automated progressive three-axis static AF demagnetization up to 200 mT, and anhysteretic remanence magnetization (ARM) acquisition were performed on a 2 G cryogenic magnetometer and Sapphire Instruments demagnetizer, respectively. ARM acquisition was performed for the purpose of measuring anhysteretic remanence anisotropy (AARM) using a three-position approach similar to *Gattacceca and Rochette* [2002]. This method is also similar to the method of measuring the anisotropy of thermoremanent magnetization taken by *Finn et al.* [2015] and the anisotropies of thermoremanent magnetization (TRM) and isothermal remanence taken by *Stephenson et al.* [1986]. A detailed description of our AARM method can be found in Document S1 in the supporting information. For most samples we used the same AF range in which the best fit line to the demagnetization was determined (see column 3 of Table S2 in the supporting information). Theoretically, this seems to be the most reasonable approach to measuring AARM with the intent of correcting remanence. However, we do not have any results that demonstrate this approach is best, and for at least one site we found this not to work well (CPT VII western sampling section). Discussion of remanence anisotropy and methods for correction of remanence, particularly with regard to CPT VII, will be the topic of a future paper. In this paper, we consider the AARM correction to improve the clustering of directions, but this does not necessarily fully restore them.

Table 1. Flow Mean Paleomagnetic Directions[a]

	Cougar Point Tuff				Sampling Location			Paleomagnetic Pole		
Ignimbrite name	*n/N*	Dec	Inc	*k*	α_{95}	Latitude	Longitude [East (+)]	Latitude	Longitude	α_{95}
CPT XVb-E	10/10	10.3	70.0	320.9	2.7	42°0.504′	−115°37.420′	76.2	270.7	4.3
CPT XIII-E	10/10	346.3	64.8	32.5	8.6	42°0.484′	−115°37.440′	79.1	184.9	12
CPT XII-E	10/10	146.0	58.6	133.0	4.2	42°0.439′	−115°37.488′			
g-CPT XII-E	10/10	147.6	52.3	369.7	2.5	42°0.439′	−115°37.488′	−9.4	271.5	2.8
CPT XI-E	16/16	147.5	−34.9	162.7	2.9	42°0.292′	−115°37.716′			
a-CPT XI-E	16/16	140.4	−46.5	223.6	2.5	42°0.292′	−115°37.716′	−54.9	323.3	2.6
CPT IX-W	8/8	215.8	19.0	225.0	3.7	42°0.430′	−115°38.205′			
CPT IX-E	10/10	220.9	25.5	243.7	3.1	42°0.285′	−115°37.787′			
CPT IX_B	18/18	218.6	22.6	369.6	1.8	-	-	−25.6	201.8	1.4
CPT VII_W	8/8	170.6	−50.9	266.4	3.4	42°0.474′	−115°38.115′			
a-CPT VII-W	8/8	177.2	−52.1	282.0	3.3	42°0.474′	−115°38.115′			
CPT VII_E	13/14	196.0	−48.0	122.0	3.8	42°0.250′	−115°38.000′			
a-CPT VII-E	13/14	191.3	−47.7	297.9	2.4	42°0.250′	−115°38.000′			
a-CPT VII-B	9/22	189.2	−50.0	344.2	2.8	-	-	−76.6	208.1	3.1
CPT V-W	8/8	241.0	81.2	415.2	2.7	42°0.555′	−115°38.124′	32.2	226.6	5.1
CPT III-W	7/7	206.1	−35.8	173.1	4.6	42°0.555′	−115°38.124′	−58.7	191.5	4.1
	Brown's Bench Escarpment				Sampling Location			Paleomagnetic Pole		
Ignimbrite name	*n/N*	Dec	Inc	*k*	α_{95}	Latitude	Longitude (Positive = East)	Latitude	Longitude	α_{95}
Rabbit Springs	9/10	1.7	70.6	88.6	5.5	42°7.693′	−115°47.898′	77.2	248.6	8.9
Jackpot	8/8	359.9	68.5	190.4	4.0	42°7.6386′	−115°47.826′	80.3	243.8	6.2
China Hill	10/10	149.7	−50.9	65.8	6.1	42°7.5996′	−115°47.741′			
a-China Hill	10/10	146.1	−54.3	132.0	4.4	42°7.5996′	−115°47.741′	−62.7	331.2	4.2
Black Canyon	12/13	216.7	23.5	131.4	3.8	42°7.476′	−115°47.716′	−26.3	203.7	2.9
Brown's Bench	14/16	198.6	−42.6	204.6	2.8	42°7.284′	−115°47.644′			
a-Brown's Bench	14/16	198.4	−45.1	260.7	2.7	42°7.284′	−115°47.644′	−68.4	194.1	2.7
Corral Creek	10/10	167.9	−37.1	89.2	5.1	42°7.207′	−115°47.628′	−66.3	273.4	4.6
BBU-1	9/9	267.3	73.6	91.7	5.4	42°15.202′	−114°15.920′			
g-BBU-1	9/9	260.4	77.9	148.3	4.2	42°15.202′	−114°15.920′	34.6	216	7.7
	Cassia Hills				Sampling Location			Paleomagnetic Pole		
Ignimbrite name	*n/N*	Dec	Inc	*k*	α_{95}	Latitude	Longitude (Positive = East)	Latitude	Longitude	α_{95}
Steer Basin	10/10	356.3	69.5	911.5	1.6	42°15.202′	−114°15.920′	78.8	234.3	2.5
Big Bluff	9/9	344.7	67.4	442.7	2.4	42°15.197′	−114°15.766′	76.8	197.9	3.6
Magpie	13/13	148.5	−43.8	117.7	3.8	42°15.057′	−114°15.843′			
a-Magpie	13/13	146.2	−44.9	133.3	3.6	42°15.057′	−114°15.843′	−58.2	316.8	3.6

[a]The ignimbrite flow mean paleomagnetic directions for the Black Rock and Brown's Bench escarpments and Cassia Mountain regions of the southern Snake River Plain. The first column shows the ignimbrite name (e.g., CPT XI). An "a-" and "g-" in front of the name (e.g., ac-CPT XI) indicates the direction was corrected using the anhysteretic remanence anisotropy (AARM) tensor and had gyroremanence removed using the SI method, respectively. An "-E," "-W," and "-B" at the end of the Cougar Point Tuff names indicate if the flow mean was obtained from the eastern (Hole in the Ground) or westernmost (southern Black Rock escarpment) subsections of the Black Rock escarpment or from both combined, respectively (e.g., CPT IX-E). For the correlation shown in Figure 2, we always use the anisotropy and gyroremanence-corrected direction if available, as well as the directions that combine results from both subsections. The second column (*n*/*N*) shows the number of sample directions used for the site-mean calculation (*n*) over the number of samples we considered using (*N*). Sample directions did not count toward the total number considered (*N*) if they were excluded either because they did not have AARM measurements or because they were vitrophyre samples that are more likely to be anisotropic. Columns 3–6 show the declination (dec), inclination (inc), precision parameter (*k*), and radius of the 95% confidence cone (α_{95}) calculated for each flow mean, respectively. Columns 7 and 8 show the latitude and longitude of the sampling site, and columns 9–11 show the latitude, longitude, and 95% confidence cone of the virtual geomagnetic pole (VGP). East is positive for all longitude values.

A customized sample handler and software [*Morris et al.*, 2009] was used for automated progressive AF demagnetization. The three-axis static alternating field demagnetization routine proposed by *Finn and Coe* [2016] was used to efficiently remove remanence from samples while accounting for gyroremanence acquisition (see section 2.2.4). Principal component analysis [*Kirschvink*, 1980] was used to calculate the best fit lines to demagnetization data, and Fisher statistics [*Fisher*, 1953] were used to calculate flow means. The paleomagnetic results from the Cassia Mountain region [*Knott et al.*, 2016a] and those for Brown's Bench were presented by *Knott et al.* [2016b]. We have reevaluated their flow mean directions (Table 1). Sample mean directions used for calculating flow mean directions can be found in Tables S1–S3.

2.2. Mitigating Pitfalls of the Paleomagnetic Analyses

2.2.1. Tectonic Rotation After Emplacement and Cooling

Any tectonic and volcano-tectonic rotation of ignimbrites after emplacement will rotate the orientation of the primary TRM directions at that site. Tectonic rotations of a single cooling unit that differ between two locations produce a discrepancy in the paleomagnetic correlation. Ignimbrites may be deposited on gently sloping surfaces [*Branney and Kokelaar*, 2002], and therefore, correcting a TRM direction simply by rotating the dip of bedding to horizontal may be inappropriate in some cases. Fortunately, at the Black Rock, Brown's Bench, and Cassia collection sections the dips of bedding are less than 5°. If the postemplacement tilting at these sections was similar to each other [see *Knott et al.*, 2016a, 2016b], then the discrepancy in directions between correlative units will be even less. Thus, the potential tectonic discrepancy is usually substantially less than the angular separation between TRM directions of stratigraphically supra-adjacent flow units. In addition, structural accounts [*Knott et al.*, 2016a, 2016b] report no strike-slip faults that would cause local vertical axis rotations.

To best avoid the potential distorting effects of tectonic rotations, we collected samples from structurally coherent (nonfaulted) stratigraphic sections. Nonetheless, the potential for differential tilting of individual eruption units within each unfaulted sections exists and may have arisen by rotation of older units prior to deposition of younger units, as recently reported [*Knott et al.*, 2016a, 2016b]. However, the excellent correlations of eruption units near the base and top of each section suggest that the effects of bedding rotations and tilting were minimal. We therefore make no attempt to correct for postemplacement tectonic disturbance of the measured paleomagnetic direction.

2.2.2. Overprint of Primary Magnetization

SR-type ignimbrites commonly contain one or more distinguishable magnetic overprints, likely from chemical, thermal, and viscous remagnetization long after initial cooling (see examples in non-SR-type ignimbrites [*Ellwood et al.*, 1989; *Reynolds*, 1977]). Magnetic overprints are generally more pronounced in weakly magnetized samples, such as those from ignimbrites with transitional polarity, and in lithoidal rather than vitrophyre sublithologies. In addition, our results from numerous cooling units show that the ignimbrite top is more susceptible to magnetic overprinting than the center and base. Preferential chemical remagnetization of the upper parts of ignimbrites elsewhere has been demonstrated and explained in detail for the Huckleberry Ridge Tuff [*Reynolds*, 1977] and Fish Canyon Tuff [*Ellwood et al.*, 1989]. For this reason, it is best to sample the basal vitrophyre and lithoidal center, although the basal vitrophyre is the most susceptible to large magnetic anisotropy, and so the lower part of the lithoidal zone should also be sampled (see section 2.2.3 below).

Figure 5 shows the orthogonal vector demagnetization ("Zijderveld") and normalized magnetization plots, as well as equal area plots of the remanence vector difference directions for samples from CPT V, CPT IX, and CPT XII. Plotting remanence vector difference directions helps one recognize identifiable components removed during a progressive demagnetization. A common magnetic overprint direction seen in many ignimbrites (Figure 4) is coincident with the southern Idaho dipole direction (declination = 0°; inclination = 60°), suggesting that it was acquired over a relatively long period of time. In addition, at least two of the ignimbrites in this study have acquired a thermochemical overprint direction close to the primary remanence direction of the overlying eruption unit. This observation suggests that emplacement of the overlying ignimbrite caused some reheating of and, possibly, mobilization of fluids within the upper part of the underlying ignimbrite. The magnetic remanence of CPT V and the upper part of CPT IX is complex, composed of three different magnetic components: (1) a high-coercivity primary TRM, (2) a low-coercivity overprint close to the dipole direction, and (3) an intermediate overprint close to the TRM direction of the overlying ignimbrite. Nonetheless, with careful demagnetization and component analysis, the direction of remanence acquired during primary cooling can almost always be found.

2.2.3. Anisotropy of Thermoremanent Magnetization

SR-type ignimbrites experience compaction strain and intense flow-related simple shear during emplacement, agglutination, and rheomorphism [*Branney and Kokelaar*, 1992]. This strain manifests as an intense mylonite-like flow fabric with associated isoclinal sheath folds (Figure 4) [*Andrews and Branney*, 2011; *Branney et al.*, 2004]. Large-remanence anisotropy develops from emplacement-related strain above both the glass transition and magnetic blocking temperatures. As a result, SR-type ignimbrites commonly have discrepant (often shallow) remanence directions rotated closer to the orientation of the shear (rheomorphic flow) direction or flattening compaction fabric [*Finn et al.*, 2015; *Gattacceca and Rochette*, 2002]. After

emplacement, devitrification begins in the ignimbrite center and migrates toward the upper and lower margins. *Finn et al.* [2015] show that crystal growth during devitrification contributes to annealing of the magnetic fabric. In general, the lithoidal center is less anisotropic and a more reliable recorder of the paleofield direction than the glassy margins, although it is still capable of having magnetic anisotropy large enough to affect the remanence. Sampling variably oriented limbs of rheomorphic folds in the lithoidal zone of the ignimbrite, typically in the upper half of thick ignimbrite sheets, may help randomize the overall effect of anisotropy on the site mean remanence direction [*Finn et al.*, 2015].

Measurement of the anisotropy of anhysteretic remanence (AARM) anisotropy was helpful in correcting for large TRM anisotropy in CPT VII and CPT XI (Figure 6). Correction using the AARM measurement improves the anisotropy-affected TRM direction but does not guarantee complete correction back to the paleofield orientation. See Document S1 for detailed description of the AARM method and results. Subblocking temperature rotation of magnetic grains has been proposed as a mechanism for shallowing remanence directions in 300 m thick welded tuff in Nevada, as indicated by curvilinear demagnetization trends [*Rosenbaum*, 1986]. However, the curvilinear demagnetization trends in the SR-type ignimbrites in the present study appear to result from a strong relationship between unblocking temperature, coercivity, remanence anisotropy, and deflection of remanence (Figure 7) [*Finn et al.*, 2015]. Subblocking temperature rotation of grains probably does not occur in the more intensely welded and rheomorphic SR-type ignimbrites since the remanence has no relationship with the steeper rheomorphic folds that develop after the compaction and flow fabric has already formed [*Andrews and Branney*, 2011; *Giessman et al.*, 2010].

2.2.4. Gyroremanence

In addition to anisotropy of TRM, the fine-grained magnetite in SR-type ignimbrites often suffers from acquisition of gyroremanence (GRM) during application of an alternating magnetic field (AF). GRM is a spurious component of magnetization that is acquired from application of an AF and can hamper attempts to demagnetize rock samples with standard three-axis static AF methods. We have found that detectable GRM is produced in most ignimbrite we have sampled, although it is more pronounced and problematic in weakly magnetized ignimbrite that cooled while the geomagnetic field was transitional (Figure 8).

The effect of GRM acquisition on a three-axis AF demagnetization is dependent on the order of axes in which the AF is applied. *Finn and Coe* [2016] present a new method for removing GRM that involves permutation of the AF axes order with progressively higher AF steps and subsequent smoothing of the resultant demagnetization data. This laboratory procedure involves no extra remanence measurements or AF applications than a typical three-axis demagnetization and, therefore, can be implemented with significant advantage as standard practice for demagnetization of rocks. In contrast, the currently accepted method for excluding GRM [*Dankers and Zijderveld*, 1981] requires two extra remanence measurements and AF applications at each progressively larger AF step and thus is rarely performed on large batches of samples. We used the permuted demagnetization routine for all samples presented in this paper and used the subsequent smoothing analysis to better component analyses for CPT XII and Brown's Bench unit (BBU)-1. Using this method to remove GRM in BBU-1 improves the correlation with CPT V (Figure 9 and Table 1). We present the unsmoothed and smoothed demagnetization data and GRM-corrected sample mean directions for both eruptive units in Tables S3 and S4.

3. Stratigraphic Correlations

3.1. Introduction

SR-type ignimbrites in the central and southwestern Snake River Plain have limited variation in major element geochemistry, and their physical features observed in the field can vary more along strike than between subsequent eruptive units (e.g., compare ignimbrites CPT XI and the China Hill Member in Figure 3). The explosive mid-Miocene volcanism that produced the Cougar Point Tuff, however, captured reversed, normal, and transitional geomagnetic field polarities (Figure 3). For this reason, characterization of the stable thermoremanence of individual cooling units can be used as a powerful correlation tool [*Bogue and Coe*, 1981; *Grommé et al.*, 1972; *Hildreth and Mahood*, 1985; *Ort et al.*, 2013; *Speranza et al.*, 2012]. In addition to polarity, volcanic sequences typically record secular changes in the geomagnetic field direction with a resolution of several hundred years [*Coe et al.*, 2005; *Hagstrum and Champion*, 2002], which is far better than the thousands to hundred thousands of year resolution achieved with radioisotopic dating techniques for rocks of this age.

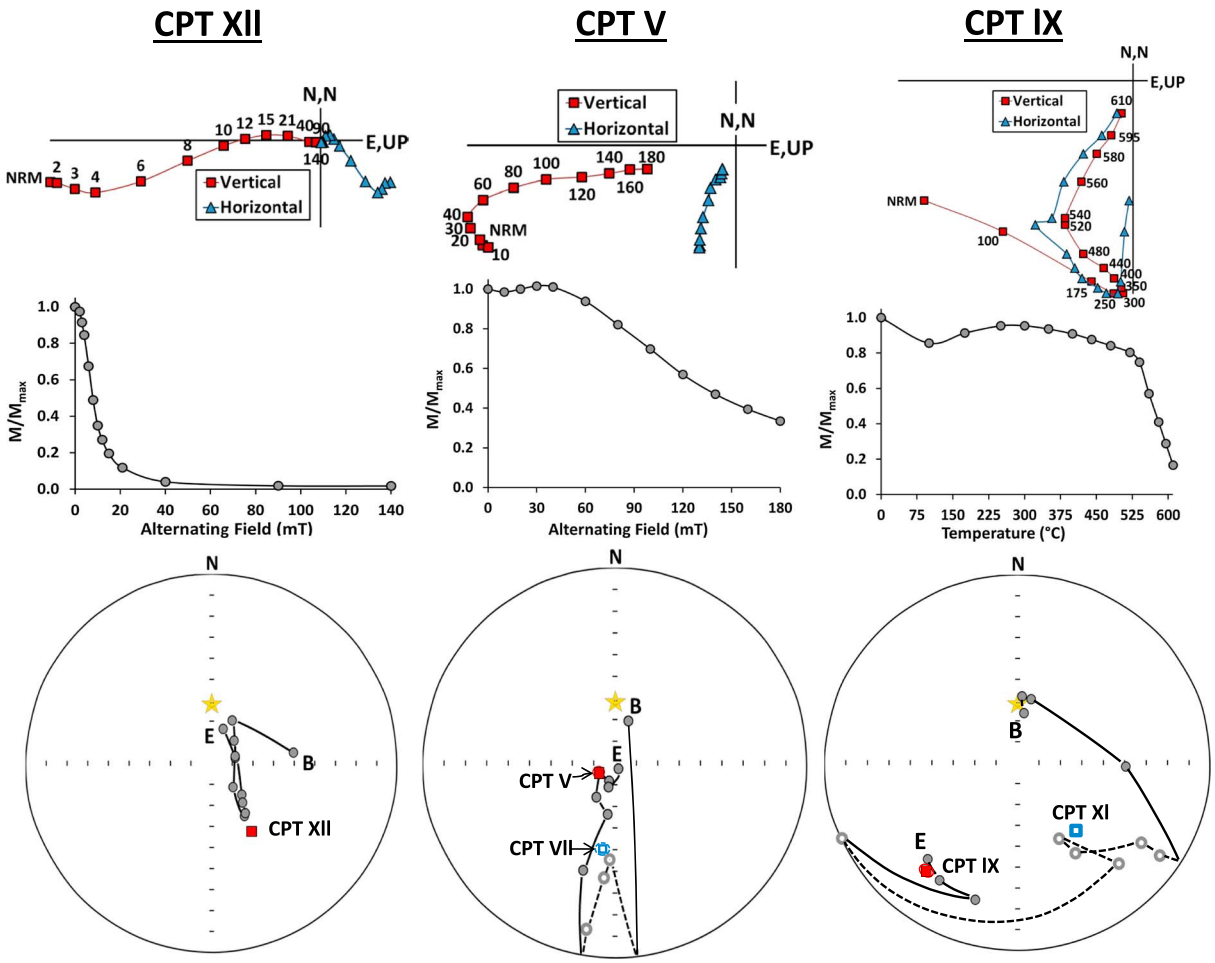

Figure 5. (previous page) Examples of magnetic overprints are shown in samples collected from the CPT V, IX, and XII ignimbrites. Zijderveld, normalized magnetization, and partial vector (i.e., vector difference) equal area equatorial net plots are shown for each sample. An AF demagnetization of a CPT XII sample has low- and high-coercivity overprints that are both close the dipole field direction. AF demagnetization of a CPT V sample and thermal demagnetization of a CPT IX contain a low-coercivity/unblocking temperature overprint close to the dipole field direction and an intermediate overprint close to the direction of the overlying flow. In all three examples, the primary remanence is successfully obtained through progressive demagnetization. The solid symbols and solid lines are lower hemisphere, and the dashed lines and hollow symbols are upper hemisphere. The red squares indicate the mean remanence direction of the ignimbrite, which the sample was collected. The blue square shows the mean direction of the overlying ignimbrite. The error circles are too small to be shown for the ignimbrite mean directions. The yellow star indicates the dipole field direction for southern Idaho. The "B" indicates the first measurement of the progressive demagnetization.

Moreover, when the field is changing rapidly during excursions and polarity reversals, the resolution can be as fine as a century or less.

The diverse remanence directions measured in the Black Rock escarpment confirm that there are at least eight separate eruption units (Figure 3). Paleomagnetic evidence for distinguishing eruption units is robust even where intervening paleosols are not exposed (e.g., CPT XI and CPT XII). In some cases (e.g., the case of CPT XIII and CPT XVb), however, magnetic remanence was not able to distinguish between what have been considered to be separate eruption units, because both units share a common field direction. In such cases, other evidence (e.g., field observations such as intervening nonwelded zones, vitrophyres, paleosols, and sediments) provided the basis for our interpretations.

This powerful paleomagnetic technique has been an exceptionally useful aid in correlation of the CPT beyond the Bruneau Jarbidge region for two reasons (Figure 3). First, the CPT records a pattern of magnetic field directions that is uncommon in Earth's history (Figures 10 and 11). The directions and corresponding virtual geomagnetic poles (Table 1) in stratigraphically adjacent flows are seldom repeated and include reversed and normal polarities and even intermediate states in two of the correlations. Second, there are multiple correlations between each ignimbrite section, and the probability that two eruption units are the same is greatly

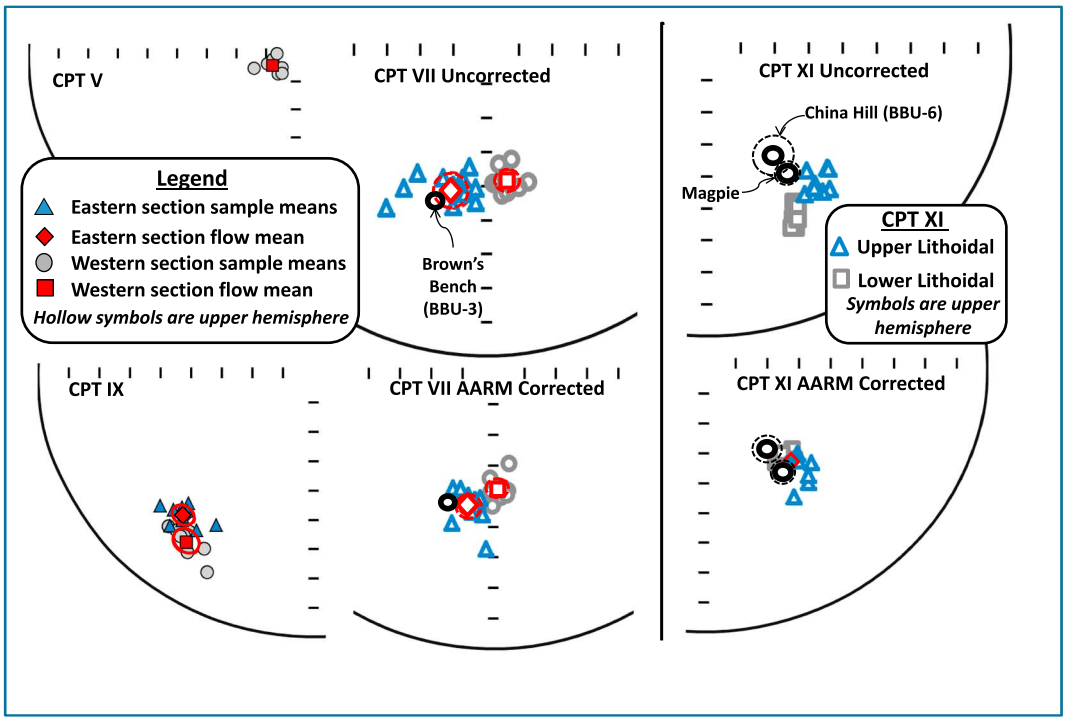

Figure 6. Equal area plots show the sample and flow mean directions for select Cougar Point Tuff (CPT) units exposed in the Black Rock escarpment. Correlative ignimbrite flow mean directions from Brown's Bench escarpment and the Cassia Mountains are plotted along with CPT VII and CPT XI sample directions that have anhysteretic remanence anisotropy (AARM) corrections. There is both tighter grouping of CPT VII sample mean directions and better agreement in between CPT XI and its correlative units after AARM corrections. The imperfect correlation between CPT VII and Brown's Bench (BBU-3) may result from one or more factors, such as magnetic anisotropy, magnetic overprinting, secular variation, and tectonic tilting.

increased if other stratigraphically correlative units also correlate paleomagnetically because the probabilities multiply [*Bogue and Coe*, 1981]. The new stratigraphic correlations are supported by geochronologic dates (Table 2) and geochemistry (Figure 12). Paleomagnetic sample mean directions are available in Tables S1–S3; description of laboratory methods, results, and plots supporting our five new ^{40}Ar-^{39}Ar dates are presented in Figures S4–S8, Document S2, and Table S5; description of the geochemical laboratory procedure is described in Document S3; and results are shown in Table S6.

The CPT correlations proposed here are only from units exposed in the Black Rock escarpment and do not include CPT X and CPT XVj, which have been reported in the Jarbidge Canyons farther to the east. CPT XV was originally mapped as one eruption unit [*Bonnichsen and Citron*, 1982] and later divided into CPT XVb and CPT XVj for their exposures in the Bruneau (Black Rock escarpment) and Jarbidge Canyons, respectively [*Perkins et al.*, 1995]. Several younger ignimbrites at Brown's Bench escarpment and in the Cassia Hills [*Knott et al.*, 2016a, 2016b] do not have correlatives within the CPT and so are not discussed in this paper.

3.2. Application of the Paleomagnetic Correlation Method of *Bogue and Coe* [1981]

We used a statistical paleomagnetic correlation method described by *Bogue and Coe* [1981] to compare the probabilities that the paleomagnetic directions of potentially correlative deposits and sequences of deposits represent either simultaneous or random samplings of the ancient geomagnetic field. P_s is the probability that two site mean directions could be as different as they are and still be erupted at the same time. Its value depends on the within-site sample dispersions of the mean directions and estimates of systematic errors that affect the mean directions (Tables 3 and 4). Potential sources of systematic error include effects from magnetic field anomalies, postemplacement tilting, uncorrected effects of anisotropy, and any unremoved overprint component. The within-site and various systematic errors are presumed to be independent and are combined to yield angular standard deviations (S) of the site-mean directions (Table 4). P_r is the probability that the site-mean directions could be as close to each other as they are and still be "random" samplings of the

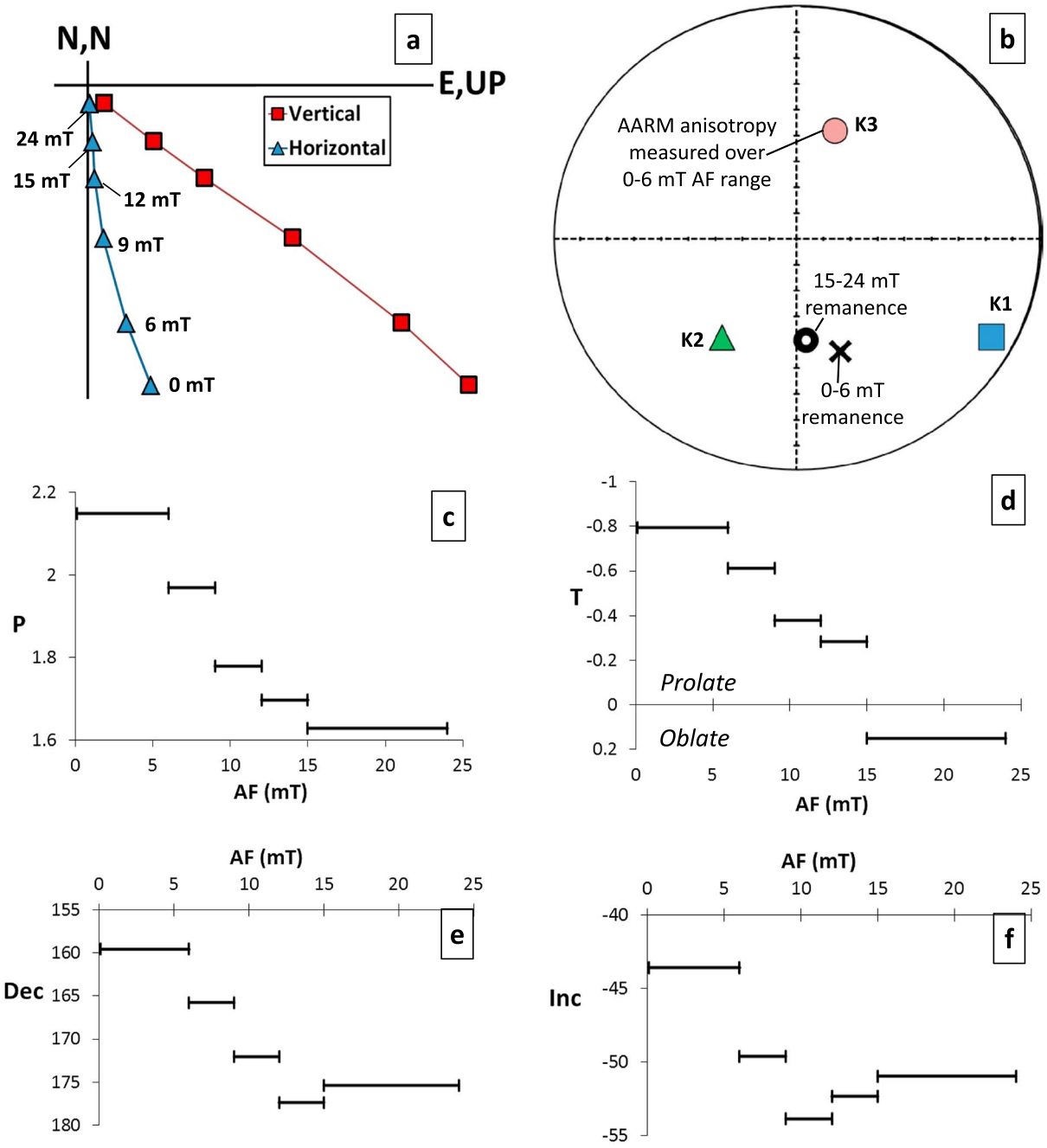

Figure 7. Magnetic remanence and partial anhysteretic anisotropy results are shown for a typical CPT VII paleomagnetic sample collected from the westernmost sampling locality at the Black Rock escarpment. The magnetic remanence was removed with very low alternating magnetic fields and has clearly been effected by a magnetic anisotropy that is particularly large and prolate at low AF levels. (a) A Zijdereld plot shows that the demagnetization trajectory is increasingly eastward and shallow with lower AF values (i.e., 0–6 mT). (b) An equal area plot shows the maximum (K_1), intermediate (K_2), and minimum (K_3) principal anhysteretic remanence susceptibility directions measured in the 0–6 mT range and the vector difference remanence directions determined from 0 to 6 mT and 15 to 24 mT. The remanence and anisotropy directions are plotted on the upper and lower hemispheres, respectively. (c–f) Plots show the dependence of several variables on AF level, including the anisotropy degree ($P = K_1/K_2$), shape factor (T), and the declination (°) and inclination (°) of the partial remanence. The horizontal bars show the AF range in which the variable on the y axis was measured. T is an anisotropy-shape parameter that describes the susceptibility ellipse shape and varies from −1 (prolate) to 1 (oblate) [*Jelinek*, 1981].

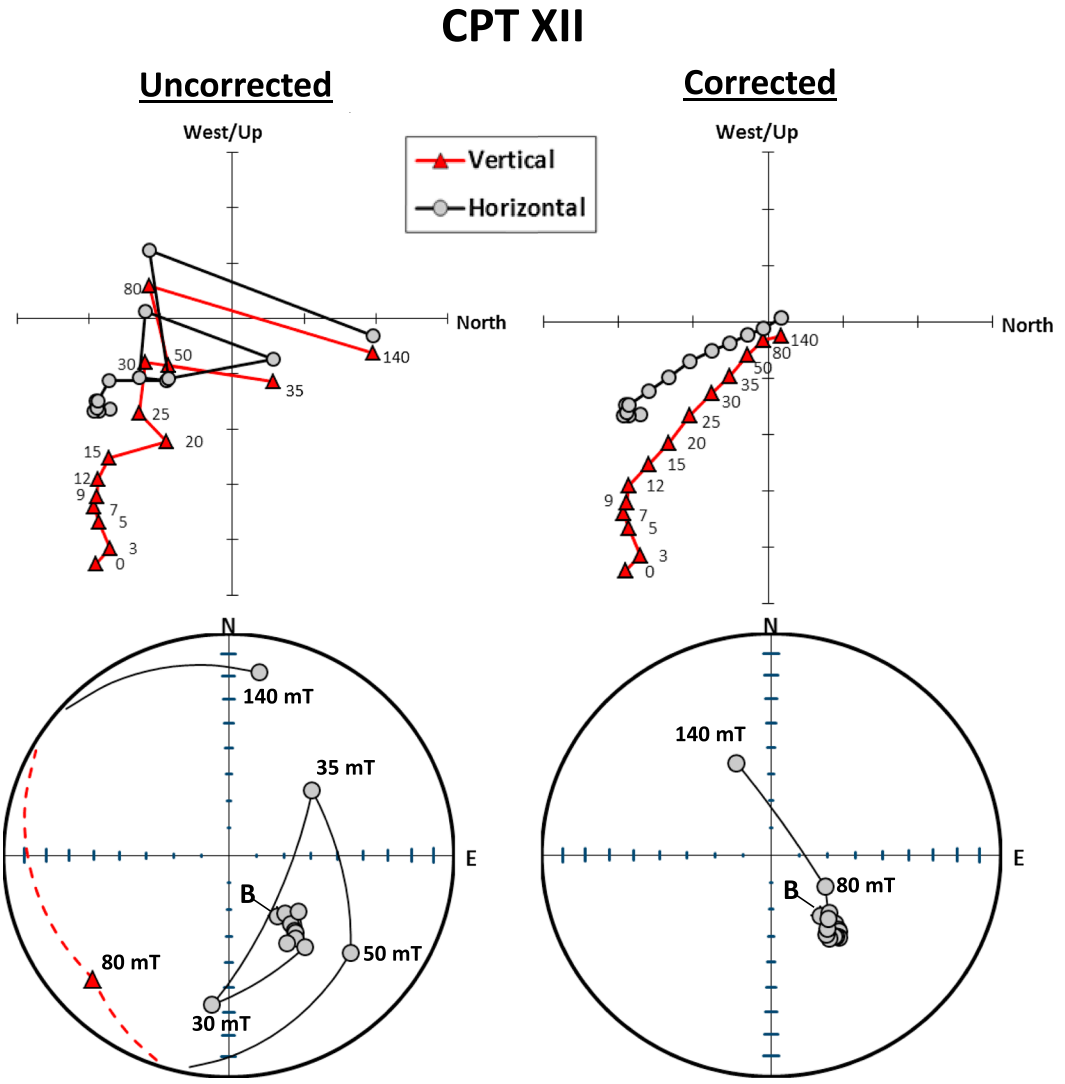

Figure 8. Zijderveld and equal area plots show the uncorrected and corrected AF demagnetization results from a sample that has a particularly large effect from gyroremanence (GRM) acquisition. The method for GRM correction is described in *Finn and Coe* [2016].

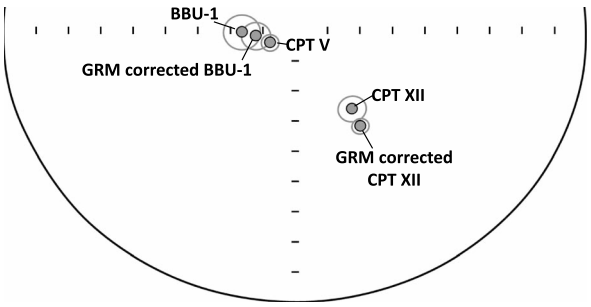

Figure 9. Equal area plots show the flow mean remanence directions determined from samples that have and have not been corrected for gyroremanence acquired during AF demagnetization. In the case of BBU-1, using the corrected samples improves the proposed correlation. In both cases the error on the site mean is reduced. The method used for correction is described in *Finn and Coe* [2016].

geomagnetic field. Its value depends on estimates of the true ancient field direction and the magnitude of its secular variation. The precision parameter (k) that best describes secular variation relevant for this study is 22.6. This value was obtained from averaging paleomagnetic directions from 108 middle to early Miocene basalt lavas in the nearby Oregon Plateau [*Jarboe et al.*, 2011]. The uniform distribution ($k = 0$), however, was used for ignimbrites CPT V and CPT IX, which apparently erupted while the geomagnetic field was in a transitional state.

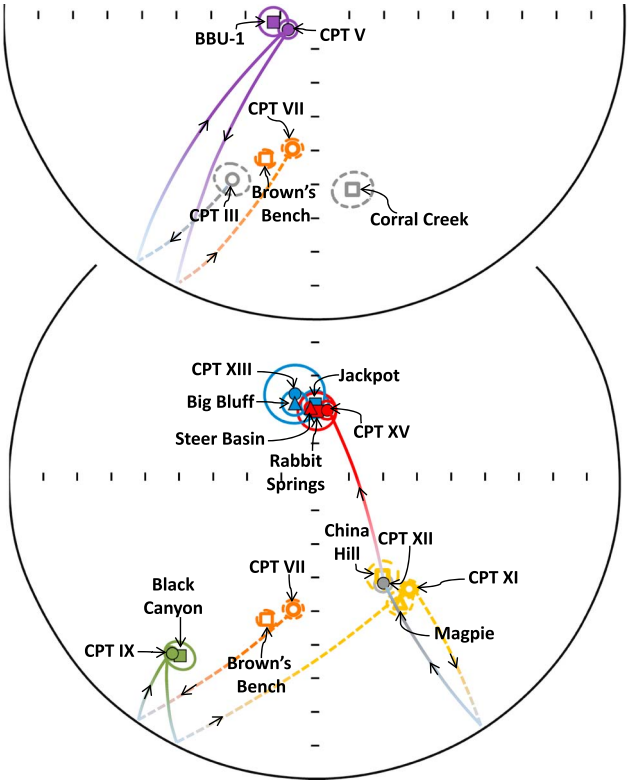

Figure 10. Equal area plots showing the paleomagnetic correlations that are color coded to match Figures 2 and 3. The grey symbols show the magnetic directions of ignimbrite which do not correlate. The hollow symbols and dashed error circles indicate upper hemisphere. The triangles are from the Cassia Mountains, and the squares and circles are from the Browns Bench and Black Rock escarpments, respectively. The lines connect the stratigraphically adjacent eruption units from the Black Rock escarpment.

The ratio of P_s to P_r is the most direct measure of whether two ignimbrites were emplaced at the same instant (Table 3). For example, a P_s/P_r ratio of 10 indicates a 10 times larger probability that the magnetic directions of the two ignimbrites were acquired at the same time rather than being spaced apart over a timespan that is long compared to secular variation. The P_s/P_r ratios for individual pairs of correlations are multiplied when considering the cumulative probability that two sections are correlative. The cumulative ratio of probabilities (P_s/P_r) for correlation between the Black Rock and Brown's Bench escarpments and between the Black Rock escarpment and Cassia Mountains are 3.8×10^{9} and 4.1×10^{4}, respectively. These extremely large values demonstrate the remarkable strength of the paleomagnetic correlations.

3.3. Discussion of Paleomagnetic Site-Mean Directions and Correlations

3.3.1. "CPT V" and "BBU-1" Units

The stratigraphically lowest correlation proposed here is between ignimbrite cooling unit CPT V at Black Rock escarpment (Figure 3) and unit BBU-1 of *Bonnichsen et al.* [2008]. BBU-1 is the rather poorly exposed, silicified, lava-like lithoidal rhyolite seen at the base of Brown's Bench escarpment, 70 km to the east of Black Rock escarpment (Figure 1). Both units record transitional geomagnetic polarity with a virtual geomagnetic pole (VGP) position located 55° from the rotation axis (Figure 11), a very unusual orientation for the geomagnetic field. The mean remanence directions of the two cooling units are only 4.8° apart, and the chance that units of very different age would both happen to capture this particular unusual field direction is about one in a thousand by the method of *Bogue and Coe* [1981]. Their P_s/P_r ratio is over 400 (Table 3).

Ignimbrite CPT V is a thin (~5 m) vitrophyric massive tuff at the sample locality on the south end of the Black Rock escarpment. Because it is thin, it probably does not have a large magnetic anisotropy, and because it lacks steep flow-banding or upright folds, any magnetic anisotropy it did have would be subhorizontal and therefore unable to significantly affect the direction of a steeply inclined remanence. The vitrophyric lithology is more resistant to magnetic overprinting and GRM acquisition than is the lithoidal lithology because SR-type vitrophyres are generally more strongly magnetic than SR-type lithoidal tuffs [*Finn et al.*, 2015], a significant advantage in this case because the geomagnetic field is unusually weak during polarity transitions. CPT V has two overprint directions that are successfully removed with magnetic cleaning (Figure 5). The low-coercivity overprint is coincident with the expected direction of the dipole field, and the intermediate-coercivity overprint matches the magnetic direction of the overlying CPT VII, which indicates that it acquired a thermochemical overprint during the subsequent eruption.

Samples from ignimbrite BBU-1 are weakly magnetized and experience significant GRM acquisition during three-axis AF demagnetization. Corrections for GRM were undertaken using the laboratory method and subsequent analysis proposed by *Finn and Coe* [2016]. The corrected flow mean remanence direction had

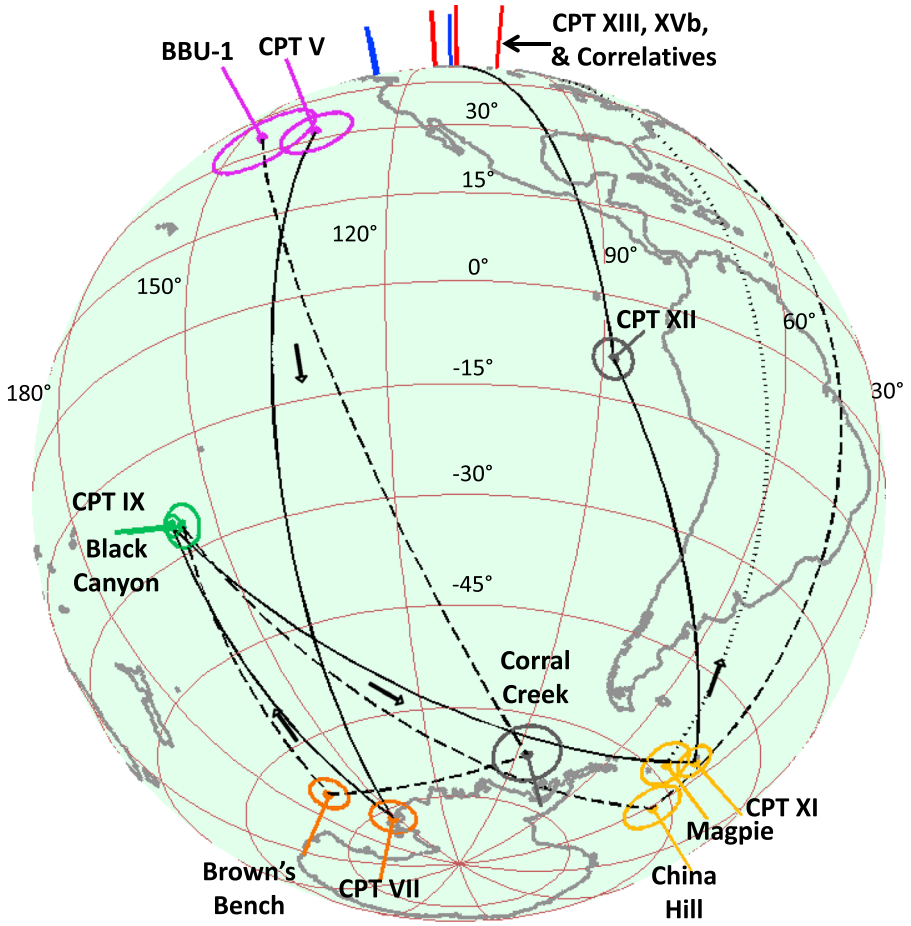

Figure 11. Plot of the Earth showing the virtual geomagnetic poles (VGPs) that are color coded to match Figures 2, 3, and 11. The lines connect the stratigraphically adjacent eruption units from the Black Rock escarpment. The solid, dashed, and dotted black lines connect the stratigraphically adjacent eruptive units in the Black Rock and Brown's Bench escarpments and Cassia Mountains, respectively. Several of the correlating VGPs have magnetic pole positions that are uncommon in Earth's history (i.e., far from the North and South Poles) and, therefore, make for very strong paleomagnetic correlations.

reduced error and was closer to the CPT V remanence direction after GRM correction (Figure 9). The correlation is further supported by XRF whole-rock compositions; in that, ignimbrites CPT V and the Brown's Bench Member both are characterized by higher silica contents (>76 wt %) compared to many other central Snake River Plain ignimbrites and low TiO_2 (≤0.3 wt %) and Sr (≤40 ppm). On a Th/Nb versus Rb/Sr plot samples of CPT V and BBU-1 fall in a separate field that does not overlap with the fields of other units (purple in Figure 12a).

3.3.2. CPT VII and Brown's Bench Member of the Rogerson Formation

The large rhyolitic explosive eruption that deposited the 11.852 ± 0.009 Ma Brown's Bench Member, Idaho, happened while Earth's magnetic field was reversed [*Knott et al.*, 2016b]. The Brown's Bench Member (formerly "BBU-3" of *Bonnichsen et al.* [2008]) is a 90 m thick lava-like outflow ignimbrite cooling unit in the Rogerson Formation characterized by a stepped erosional profile and compositionally distinct population of augites and two pigeonites [*Knott et al.*, 2016b].

The site-mean magnetic directions for CPT VII at Black Rock escarpment, and for the Brown's Bench Member, ~70 km to the east, are just 7.9° apart and the P_s/P_r ratio is 3.8 (Table 3). The Corral Creek Member, an ignimbrite cooling unit that directly underlies the Brown's Bench Member, also records reverse polarity, but its site-mean direction is more than twice as far from that of CPT VII, and the resulting P_s/P_r ratio is 200 times smaller. Moreover, our new high-precision geochronologic dates (Figure 2 and Table 2) for CPT VII (11.855 ± 0.006 Ma) and the Brown's Bench Member (11.852 ± 0.009 Ma) strongly support the correlation

Table 2. Summary of Radioisotopic Dates on Sanidine Crystals for Members of the Cougar Point Tuff and Rogerson and Cassia Formations with Sample Locations, Material Type, and Method Used[a]

Member	Sample Location	Method	Weighted Mean Age (Ma)	Inverse Isochron Age (Ma)	MSWD	$^{40}Ar/^{36}Ar$
Cougar Point Tuff XIII	Bruneau Canyon	Single-grain laser fusion	10.92 ± 0.06[b]	-		
Jackpot	Brown's Bench escarpment	Single-grain laser fusion	10.960 ± 0.009[c]	10.960 ± 0.013[c]	1.0	294 ± 15
Big Bluff	Cassia Hill	Single-grain laser fusion	10.97 ± 0.07[d]	-		
Cougar Point Tuff XI	Jarbidge Canyon	Single-grain laser fusion	11.35 ± 0.07[b]	-		
China Hill Member	Brown's Bench escarpment	Single-grain laser fusion	11.305 ± 0.016[e]	11.32 ± 0.02[e]	0.3	295 ± 7
Magpie Basin	Cassia Hill	Single-grain laser fusion	11.337 ± 0.008[f]	11.336 ± 0.009[f]	1.0	294 ± 11
Cougar Point Tuff IX	Bruneau Canyon	Single-grain laser fusion	11.70 ± 0.07[b]	-		
Black Canyon	Corral Creek (upper vitrophyre)	Single-grain laser fusion	11.667 ± 0.017[c]	11.66 ± 0.02[c]	0.8	299 ± 6
Black Canyon	Corral Creek (basal vitrophyre)	Single-grain laser fusion	11.662 ± 0.009[e]	11.658 ± 0.016[e]	1.0	303 ± 18
Cougar Point Tuff VII	Deer Creek grade	Single-grain laser fusion	11.852 ± 0.007[e]	11.854 ± 0.008[e]	1.0	297 ± 4
Browns Bench	Brown's Bench escarpment	Single-grain laser fusion	11.852 ± 0.009[e]	11.845 ± 0.014[e]	1.0	310 ± 20
Cougar Point Tuff V	Murphey Hotsprings	Single-grain laser fusion	12.288 ± 0.014[e]	12.287 ± 0.018[e]	2.0	299 ± 1
Cougar Point Tuff III	Bruneau Canyon	Single-grain laser fusion	12.81 ± 0.08[b]	-		

[a]All argon ages are relative to sanidine feldspar standard FCs at 28.172 Ma ± 0.028 Ma [*Rivera et al.*, 2011] and reported with 2 s uncertainties.
[b]*Bonnichsen et al.* [2008].
[c]*Knott et al.* [2016b].
[d]*Ellis et al.* [2012].
[e]This study (Table S5).
[f]*Knott et al.* [2016a].

we propose. This interpretation is also supported by whole-rock geochemistry; in that, both CPT VII and the Brown's Bench Member share some distinctive features: Rb/Sr ratios are low (<4), and the SiO_2 (72.4–73.0 wt %) and TiO_2 values (~0.52 wt %) are lower than in many other central Snake River Plain ignimbrites (orange in Figure 12a). In terms of mineralogy, both CPT VII and Brown's Bench Member contain three fairly distinctive pigeonite populations (Figure 12b). Two of these three pyroxene compositions also occur in CPT III, and the pyroxene population differs significantly from that of CPT IV.

Ignimbrite cooling unit CPT VII was sampled at two locations (<1 km apart) at the Black Rock escarpment (Figure 1), and there is a moderate discrepancy (4.3°) between the two remanence directions (Figure 6). The magnetic anisotropy was generally large for many samples, and the anhysteretic remanence anisotropy (AARM) corrections only partly resolved this discrepancy. The magnetic anisotropy and remanence in the lithoidal samples are held by grains that have a low coercivity, particularly in the westernmost sampling location on the southern end of the Black Rock escarpment. The larger amount of remanence focused in this highly anisotropic low-coercivity range (Figure 7) complicates the AARM correction. Since this correction is only partly successful for this ignimbrite, we excluded highly anisotropic samples from flow mean analysis with a ratio (P) of maximum (K_1) to minimum (K_3) principal susceptibility directions of greater than 1.5. In contrast to CPT VII, samples of the Brown's Bench Member have well-clustered paleomagnetic directions and low-remanence anisotropy, suggesting that the site-mean magnetic direction is of high quality.

3.3.3. CPT IX and the Black Canyon Member of the Rogerson Formation

The CPT IX and the Black Canyon Member [*Knott et al.*, 2016a] (formerly "BBU-4 and BBU-5" of *Bonnichsen et al.* [2008]) erupted while Earth's magnetic field had a transitional direction with the VGP almost 65° from the rotation axis (Figure 11). Their site-mean directions are not significantly different (only 2° apart), which makes for a very strong paleomagnetic correlation (P_s/P_r ratio = 3085.5; Table 3). Supporting this correlation, CPT IX and the Black Canyon Member also have similar trace element chemistry (Figure 12a) and indistinguishable pigeonite compositions (Figure 12b), although the compositionally distinct augites present in the Black Canyon Member were not reported from CPT IX.

We have not measured magnetic anisotropy of CPT IX and the Black Canyon Member but suspect that it has had little effect because the sample directions are tightly clustered and the site means agree well. CPT IX and the Black Canyon Member both have significant magnetic overprinting in their upper parts (Figure 5). We therefore do not present any paleomagnetic results from samples collected from there nor use them for determination of the ignimbrite mean directions. Paleomagnetic sites were collected stratigraphically lower within each ignimbrite that are far less affected by magnetic overprinting.

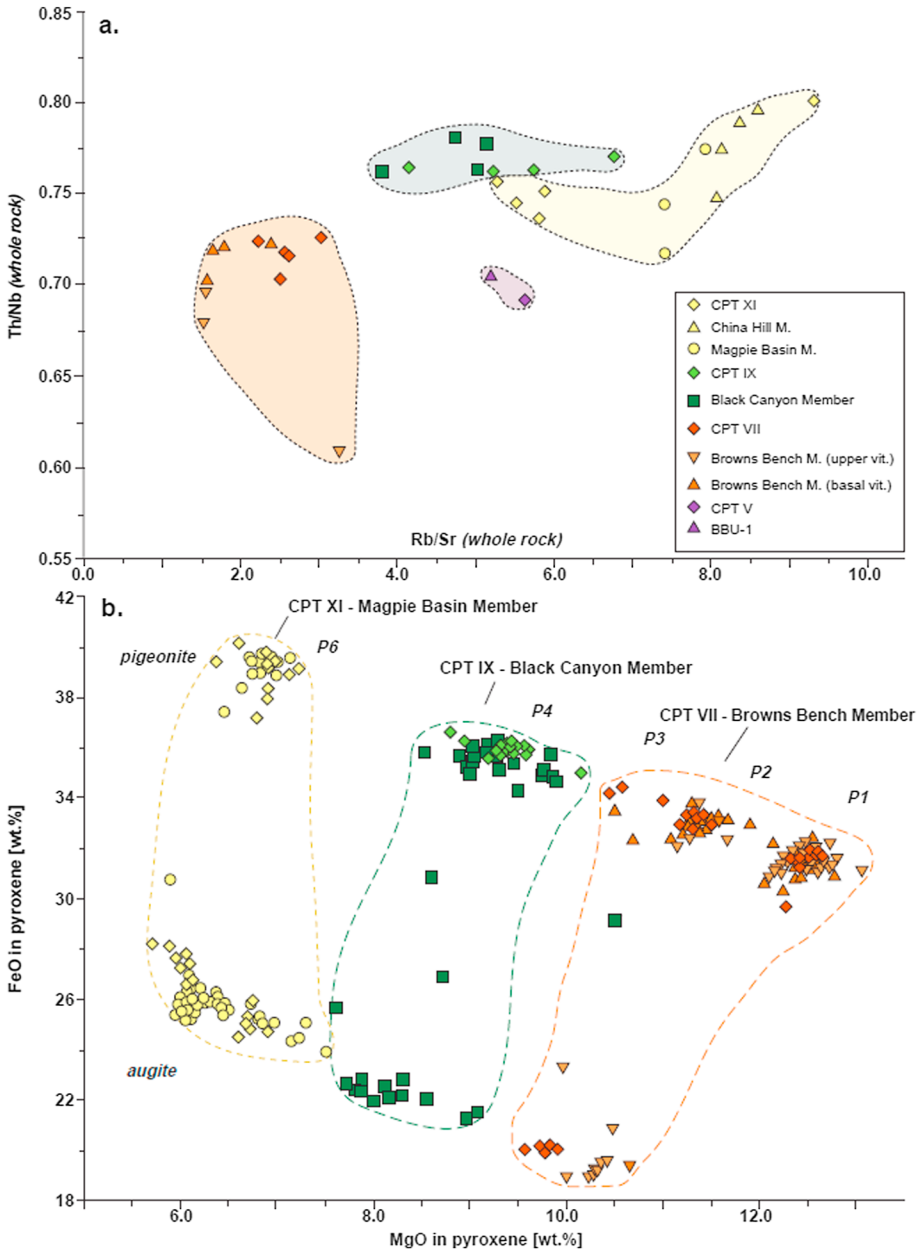

Figure 12. (a) Rb/Sr versus Th/Nb whole-rock element ratios. (b) FeO versus MgO (wt %) in SRP pigeonite and augite showing overlapping augite and pigeonite composition of the proposed correlation. Modal pigeonite composition P1–4 and P6 and CPT XI pyroxene data are after *Cathey and Nash* [2004].

3.3.4. CPT XI, the China Hill Member (Rogerson Formation), and the Magpie Basin Member (Cassia Formation)

The CPT XI eruption occurred during a time when Earth's magnetic field was reversed, and its VGP positioned ~30° away from the rotation axis is relatively unusual. The magnetic directions of the China Hill Member of the Rogerson Formation at Brown's Bench (Figure 1; former BBU-6 of *Bonnichsen et al.* [2008]) and of the Magpie Basin Member of the Cassia Formation are 8.6° and 4.4° from that of CPT XI, respectively, and 9.4° from each other. The P_s/P_r ratios describing the correlation of CPT XI with Magpie and China Hill are 100.1 and 4.6, respectively (Table 3). Available ^{40}Ar-^{39}Ar geochronologic dates of sanidine crystals from CPT XI (11.35 ± 0.07 Ma [*Bonnichsen et al.*, 2008]) and from the Magpie Basin Member (11.337 ± 0.008 Ma [*Knott et al.*, 2016a]) agree within error. We present a new weighted mean sanidine ^{40}Ar-^{39}Ar age of 11.305 ± 0.016 Ma for the China Hill Member (Table 2). Although this age is slightly younger the

Table 3. Flow by Flow Correlations[a]

Site Pairs	k	δ	α	P_r	P_s	P_s/P_r	Cum P_s/P_r
CPT XVb-E	335.9	9.7	3.0	2.24E − 02	0.83	37.1	3.71E + 01
Rabbit Springs	234.6	9.4					
CPT XIII-E	165.4	7.2	6.5	1.14E − 01	0.53	4.6	1.72E + 02
Jackpot	244.9	7.3					
a-CPT XI-E	408.2	27.0	8.6	5.02E − 02	0.23	4.6	7.90E + 02
a-China Hill	194.7	19.1					
CPT IX_B	245.6	89.4	2.0	3.04E − 4[b]	0.94	3085.5	2.44E + 06
Black Canyon	195.0	90.3					
a-CPT VII-B	207.7	12.3	7.9	9.12E − 02	0.35	3.8	9.28E + 06
a-Brown's Bench	240.5	19.4					
CPT V-W	239.0	33.9	4.8	1.8E − 3[b]	0.73	417.6	3.87E + 09
g-BBU-1	141.4	32.9					
CPT XVb-E	335.9	9.7	4.9	6.05E − 02	0.55	9.2	9.16E + 00
Steer Basin	320.8	8.4					
CPT XIII-E	165.4	7.2	2.7	1.98E − 02	0.89	45.1	4.13E + 02
Big Bluff	271.9	9.0					
a-CPT XI-E	245.6	27.0	4.4	6.73E − 03	0.67	100.1	4.14E + 04
a-Magpie	308.4	25.6					

[a]Ignimbrite by ignimbrite correlation statistics of the Cougar Point Tuffs, following the method of *Bogue and Coe* [1981]. k is the precision parameter for the estimated uncertainty in the ignimbrite mean direction from Table 4; δ is the angular distance between the paleomagnetic and axial dipole direction; α is the angle between the two paleomagnetic directions; P_r is the probability of the random hypothesis that the two ignimbrites could have been erupted independently at times far apart compared to the time scale of paleomagnetic secular variation and yet have directions as close to each other as they are; P_s is the probability of the simultaneous hypothesis that the two ignimbrites could have been emplaced at the same time and yet have directions that are as far apart from each other as they are; P_s/P_r is the probability ratio that indicates most directly the relative likelihood that the two ignimbrites erupted at the same time rather than have similar directions by chance; and "cum P_s/P_r" is the cumulative probability for considerations of multiple correlations, starting with the youngest and sequentially including older ignimbrites.

[b]Uniform distribution ($k = 0$) used because full-polarity Fisher distribution does not apply for transitional directions. Cumulative P_s/P_r would be ~30 times greater if Fisher distribution with $k = 22.6$ was used.

Table 4. Paleomagnetic Data and Uncertainties[a]

Site	k	$\bar{S}_W$	$\bar{S}_F$	$\bar{S}_T$	$\bar{S}_A$	$\bar{S}_O$	$\bar{S}$	$\bar{k}$
				Cougar Point Tuff				
CPT XVb-E	320.9	1.4	0.5	2.0	3.5	1.0	4.4	335.9
CPT XIII-E	32.5	4.5	0.5	2.5	3.0	2.0	6.3	165.4
a-CPT XI-E	223.6	1.4	0.5	3.0	2.0	1.0	4.0	408.2
CPT IX_B	369.6	1.0	0.5	3.5	3.5	1.0	5.2	245.6
a-CPT VII-B	344.2	1.5	0.5	4.0	3.5	1.0	5.6	207.7
CPT V-W	415.2	1.4	0.5	4.5	2.0	1.0	5.2	239.0
				Brown's Bench escarpment				
Rabbit Springs	88.6	2.9	0.5	2.5	3.5	1.0	5.3	234.6
Jackpot	190.4	2.1	0.5	3.0	3.5	1.0	5.2	244.9
a-China Hill	132.0	2.2	0.5	3.5	3.5	2.0	5.8	194.7
Black Canyon	131.4	2.0	0.5	4.0	3.5	1.0	5.8	195.0
a-Brown's Bench	260.7	1.3	0.5	4.5	2.0	1.0	5.2	240.5
g-BBU-1	148.3	2.2	0.5	5.0	3.5	2.0	6.8	141.4
				Cassia Hills				
Steer Basin	911.5	0.8	0.5	2.5	3.5	1.0	4.5	320.8
Big Bluff	442.7	1.3	0.5	3.0	3.5	1.0	4.9	271.9
a-Magpie	133.3	1.9	0.5	3.5	2.0	1.0	4.6	308.4

[a]The errors are shown related to the uncertainty involved in determination on flow mean remanence directions. k is the *Fisher* [1953] precision parameter describing the within-site dispersion of sample directions; $\bar{S}_W$ is the associated angular standard deviation of the mean in degrees; $\bar{S}_T$, $\bar{S}_A$, and $\bar{S}_O$ are the assigned angular standard deviations in degrees of the flow mean direction due to postemplacement tectonic tilts and rotations, magnetic field anomalies, uncorrected magnetic anisotropy, and unremoved magnetic overprints, respectively; $\bar{S}$ is the combined error due to the four uncertainties assuming that they are independent; and $\bar{k}$ is the precision parameter associated with $\bar{S}$.

correlating inverse isochron age of 11.324 ± 0.020 Ma is indistinguishable from the published ages for the Magpie Basin Member and CPT XI unit.

This newly correlated ignimbrite is thickest at the Black Rock escarpment (CPT XI) and where we also have measured the largest AARM. In contrast to CPT VII, many of the anisotropic samples from this location have remanences carried by high-coercivity grains. The AARM corrections (as described above) work very well in improving the paleomagnetic correlation, probably because the remanence resides in a coercivity range where the AARM is easily measured. The AARM of CPT XI samples, in contrast to that of CPT VII, seems to be able to completely correct the most anisotropic samples from this flow, and so we do not exclude samples based on the magnitude of *P*.

The China Hill and Magpie Basin Members have a much smaller though not insignificant degree of anisotropy. We measured anisotropy for most but not all samples from the two. Unfortunately, we destroyed many samples for geochemical analysis before realizing that magnetic anisotropy would present a problem. To be consistent, however, we include all samples in calculation of the ignimbrite mean directions for each location. These ignimbrite mean directions do not change too much if uncorrected samples are excluded since they probably had only moderate to low anisotropy.

Whole-rock geochemistry lends support to the correlation between CPT XI, the China Hill Member, and the Magpie Basin Member. They all have unusually low TiO_2 contents (<0.26 wt %) and occupy the same field on the Th/Nb versus Rb/Rr plot (Figure 13a Geochem) and have Rb/Sr ratios between 5.2 and 9.5. In contrast, the underlying Black Canyon Member displays Rb/Sr ratios ≤5.2. Pyroxene compositions are also distinct from those of underlying units, with higher (>38 wt %) FeO (pigeonites >38 wt %; augites >24 wt %) and lower MgO contents (6–7 wt %; Figure 12b).

A correlation between CPT XI and the Black Canyon Member of the Rogerson Formation (former BBU-5 of *Bonnichsen et al.* [2008]) has been proposed [*Ellis et al.*, 2012]. However, this proposed correlation is inconsistent with our results that show the paleomagnetic directions of CPT XI to differ from that of the Black Canyon Member but to closely resemble those of the China Hill and Magpie Basin Members. Moreover, the compositions of both pigeonites and augites within the Magpie Basin Member are significantly different to those in the Black Canyon Member (Figure 12b). At Brown's Bench escarpment, the China Hill Member underlies the Black Canyon Member (Figures 2 and 3), for which *Ellis et al.* [2012] report an ^{40}Ar-^{39}Ar date of 11.41 ± 0.08 Ma (recalculated to *Rivera et al.* [2011]). This age is much closer to our new China Hill Member ^{40}Ar-^{39}Ar date of 11.305 ± 0.016 Ma than it is to ages derived from samples collected from the base and top of the Black Canyon Member. It is possible that *Ellis et al.* [2012] unknowingly sampled the China Hill Member instead of the Black Canyon Member.

3.3.5. Correlations to CPT XIII and CPT XVb

The CPT XIII unit is tied to the Rabbit Springs unit (at Brown's Bench) and the Steer Basin unit (at Cassia Hills) by its stratigraphic position, similar plagioclase and augite compositions [*Ellis et al.*, 2012], and radioisotopic dates that are indistinguishable within error (Figure 2). The CPT XVb unit is tied to the Jackpot unit (at Brown's Bench) and Big Bluff unit (as Cassia Hills) by its stratigraphic position, similar clinopyroxene and whole-rock compositions, and similar physical characteristics (*Perkins et al.*, 1995; *Ellis et al.*, 2012]. Radioisotopic data show that these likely correlatives at Brown's Bench and the Cassia Mountains are separate cooling units spaced in time by ~0.35 Myr (Figure 2 and Table 2) [*Bonnichsen et al.*, 2008; *Ellis et al.*, 2012]. All this evidence supports previous suggestions [e.g., *Bonnichsen and Citron*, 1982; *Ellis et al.*, 2012] that CPT XIII and CPT XVb represent separate eruption units.

The similar geomagnetic field direction that the CPT XIII and CPT XVb units have recorded is not particularly unusual but in the absence of other evidence would suggest that the two units erupted at nearly the same time. In this case, however, it is clear that similarity is simply fortuitous (as is the similarity of the Rabbit Springs and Jackpot directions at Brown's Bench and the similarity of the Steer Basin and Big Bluff directions at Cassia Hills). To assess the stratigraphic correlation, what matters is the similarity of directions between CPT XIII and its correlatives combined with the similarity of directions between CPT XVb and its correlatives. Those comparisons yield cumulative P_s/P_r ratios of 172 and 413, respectively. The combined paleomagnetic, geochronologic, and geochemical evidence; physical characteristics; and relative stratigraphic positions adjacent to other correlative ignimbrites strongly support the previous suggestion by *Ellis et al.* [2012] that these six widely spaced deposits represent two eruptions.

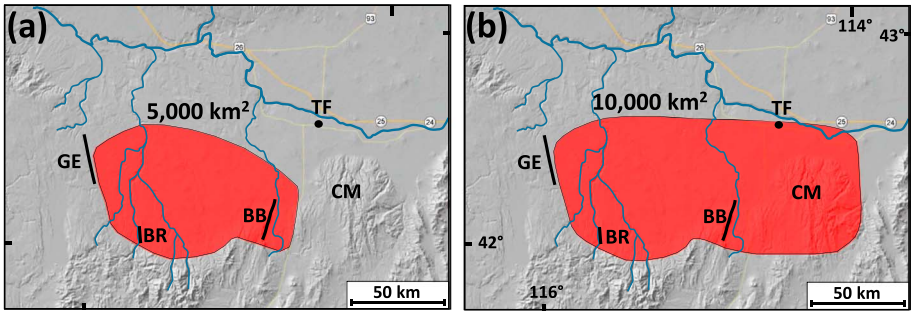

Figure 13. Estimates of the extent of deposition of eruptions that correlate between the Black Rock escarpment (BE), Brown's Bench (BB), and Cassia Mountains (CM). (a) The estimated areas for CPT V, VII, and IX are shown and (b) areas for CPT XI, XIII, and XVb are also shown. The Grasmere escarpment (GE) ignimbrite is considered part of the CPT, although because of the uncertainty in how it correlates with the CPT units with roman numerals, it is not included in the areal extent.

4. New Cougar Point Tuff Eruption Area and Volume Estimates

4.1. Cougar Point Tuff Volume Estimation Methods and Results

Individual CPT ignimbrite sheets thicken northward toward their inferred source in the southern Snake River Plain, where they are concealed by younger basalts [*Bonnichsen and Citron*, 1982]. They also likely extend farther south beyond the Snake River Plain along paleovalleys, have thick caldera fills of unknown dimensions, and widely dispersed ashfall components. CPT thickness distributions are poorly known as they are primarily exposed in widely spaced canyons and escarpments. For the reasons listed above, individual CPT eruption volumes can only be estimated with an accuracy slightly better than an order of magnitude. Method 2 from *Ellis et al.* [2012] is used here for volume estimation. This procedure involves (1) estimation of the aerial extent, (2) multiply the area by the average thickness, (3) double the volume to account for caldera infill, and (4) ignore the ashfall component.

Figure 13 shows the general areas of deposition for CPT units exposed in the Black Rock and Brown's Bench escarpments (CPT V, VII, and IX) and those that occur farther east to the Cassia Mountains (CPT XI, XIII, and XVb). These aerial extents of 5000 km^2 and 10,000 km^2, respectively, are rough estimates and should be treated as tentative. The average thicknesses used for each CPT are taken as the average of the minimum and maximum observed thicknesses (min-max, avg): CPT V (10–40 m, 30 m), CPT VII (40–100 m, 70 m), CPT XI (20–100 m, 60 m), CPT XIII (20–100 m, 60 m), and CPT XVb (20–100 m, 60 m). Following the method of *Ellis et al.* [2012], minimum volume estimate of CPT V is 300 km^3; CPT VII is 700 km^3; CPT IX is 400 km^3; and CPT XI, XIII, and XVb are 1200 km^3.

4.2. Aerial Extent of the Newly Expanded Cougar Point Tuff

South of the towns of Jackpot, Jarbidge, and Rowland Nevada, the SRP Miocene welded tuffs are discontinuously covered by late Miocene sediments [*Bushnell*, 1967; *Sharp*, 1939] and onlap the 15–17 Ma pre-Snake River Plain Jarbidge rhyolite, Jurassic to Cretaceous granites, and marine strata of mostly Permian and Pennsylvanian age [*Bonnichsen and Citron*, 1982; *Coats*, 1987]. The southern extent of the CPT and its correlatives are drawn conservatively in Figure 13 along the southernmost continuous exposure of SRP Tuffs [*Coats*, 1987]. There are discontinuous exposures of SRP Tuffs farther south in northern Nevada, but there are fewer individual cooling units and direct correlations are unknown. The western margin of the Bruneau-Jarbidge eruptive center is thought to be marked by the Grasmere escarpment, where at least three Cougar Point Tuffs are exposed (Figure 13). The youngest of the three, the Grasmere escarpment ignimbrite, is thought to be correlative to CPT XI based on age, geochemistry, and magnetic polarity [*Bonnichsen et al.*, 2008]. However, there is not enough evidence to include this deposit as part of the same eruption that produced the CPT XI, and for this reason, the Grasmere escarpment is used here as a western border of all the CPT units.

The CPT units that are exposed in Brown's Bench escarpment are also inferred to underlay the immediately adjacent low-lying Rogerson Graben to the east, and those that occur even farther east are inferred to be present throughout the Cassia Mountains. This may be a small overestimate for CPT XI, which likely only occur as

an ashfall deposit in the far eastern Cassia Mountains. The extent of the CPT units to the north in the Snake River, where they are concealed by younger basalt flows, is by far the boundary with the largest uncertainty. The northern margin is conservatively extended into the plain in Figure 13, although the exact location of the northern extent of most CPT eruptions is entirely unknown. It is likely that some of the CPT units are present on the far northern margin of the Snake River Plain, which will be the focus of a future paper.

5. Discussion and Conclusion

The magnetic remanence preserved in strongly welded and rheomorphic ignimbrites is a powerful tool for (a) distinguishing between the products of separate explosive volcanic eruptions and (b) for stratigraphic correlation of defined eruption units. The technique is best employed together with field data, whole-rock and mineral chemistry, and radioisotopic dating. However, because the timespans represented by error bars in even high-resolution radioisotopic dating, as presented in this paper, are of sufficient duration to host more than one large explosive eruption, radioisotopic dating can be more readily employed to disprove a volcanostratigraphic correlation, rather than to establish one. Thus, paleomagnetic correlation is the only method with temporal resolution (a few centuries) capable of determining with confidence if multiple ignimbrite deposits were simultaneously emplaced. The combined use of these temporal constraints with geochemical characterization addresses the two fundamental criteria used for correlating deposits from individual eruption events: they share the same magma source and were emplaced simultaneously. Using these techniques we have demonstrated, with confidence, that most of the Cougar Point Tuff extends occur in the Brown's Bench escarpment and some even farther east to the Cassia Mountains. The correlations presented here demonstrate that mid-Miocene Yellowstone hot spot eruptions were much larger and infrequent than previously thought.

We propose a new protocol to mitigate potential pitfalls that could yield incorrect determinations of magnetic remanence directions in SR-type ignimbrites and which we expect will be helpful in paleomagnetic studies of partly glassy silicic lavas and rheomorphic ignimbrites elsewhere. We recommend collecting paleomagnetic samples at two sites from each cooling unit: one from the stable and more strongly magnetized basal vitrophyre, which is more resistant to chemical overprinting, and the other from the rheomorphically folded devitrified central part of the ignimbrite, as this is least affected by magnetic anisotropy and relatively far from the chemical remanent magnetization-prone ignimbrite top. The measurement of anhysteretic remanence anisotropy can be used to detect and at least partly correct the effects of large thermal remanence anisotropy, and a new protocol for three-axis AF demagnetization [*Finn and Coe*, 2016] can be used to avoid potentially interfering effects of gyroremanence (GRM). This protocol takes no extra time or effort and therefore should be implemented as a matter of course. If GRM is then found to be problematic after the demagnetization experiment, a subsequent smoothing analysis may be used to remove the unwanted GRM effects (e.g., as was applied to BBU-1 and CPT XII).

Acknowledgments

Expenses for this work were covered by the Natural Environment Research Council grant NE/G005372/1 awarded to Michael Branney. Quadlab is funded by a grant to Michael Storey from the Villum Foundation. The salary and school fees for the first author (D.F.) were covered in part by a National Science Foundation grant (EAR 1250444) awarded to X. Zhao. D.F. would also like to thank the University of California, Santa Cruz for providing >20 teaching assistant and primary instructor positions, which enabled completion of the work presented in this paper. We also would like to thank Grant Rhea-Downing for his assistance with paleomagnetic field sampling and discussion on magnetic anisotropy and the Bureau of Land Management for the assistance with field work logistics. Finally, we are indebted to Scott Bogue and Bernard Henry whose reviews and comments helped us significantly improve this paper. Please contact the first author via e-mail at dfinn@ucsc.edu for data requests and other questions.

References

Andrews, G. D., and M. J. Branney (2011), Emplacement and rheomorphic deformation of a large, lava-like rhyolitic ignimbrite: Grey's Landing, southern Idaho, *Geol. Soc. Am. Bull.*, *123*(3-4), 725–743.

Armstrong, R. H. L., W. P. Leeman, and H. E. Malde (1975), K-Ar dating Quaternary and Neogene volcanic rocks of the Snake River Plain, Idaho, *Am. J. Sci.*, *275*(3), 225–251.

Armstrong, R. L., J. E. Harakal, and W. M. Neill (1980), K-Ar dating of Snake River Plain (Idaho) volcanic rocks—New results, *Isochron West*, *27*, 5–10.

Bindeman, I. N., and A. G. Simakin (2014), Rhyolites–hard to produce, but easy to recycle and sequester: Integrating microgeochemical observations and numerical models, *Geosphere*, *10*, 930, doi:10.1130/GESOO969.1.

Bogue, S. W., and R. S. Coe (1981), Paleomagnetic correlation of Columbia River basalt flows using secular variation, *J. Geophys. Res.*, *86*, 11,883–11,897, doi:10.1029/JB086iB12p11883.

Bonnichsen, B., and G. P. Citron (1982), The Cougar Point Tuff, southwestern Idaho and vicinity, in *Cenozoic Geology of Idaho*, *Idaho Bur. of Mines and Geol. Bull.*, vol. 26, pp. 255–281.

Bonnichsen, B., W. P. Leeman, N. Honjo, W. C. McIntosh, and M. M. Godchaux (2008), Miocene silicic volcanism in southwestern Idaho: Geochronology, geochemistry, and evolution of the central Snake River Plain, *Bull. Volcanol.*, *70*(3), 315–342.

Branney, M. J., and P. Kokelaar (1992), A reappraisal of ignimbrite emplacement: Progressive aggradation and changes from particulate to non-particulate flow during emplacement of high-grade ignimbrite, *Bull. Volcanol.*, *54*(6), 504–520.

Branney, M. J., and B. P. Kokelaar (2002), Pyroclastic density currents and the sedimentation of ignimbrites, *Geol. Soc. of London*.

Branney, M. J., T. L. Barry, and M. Godcheaux (2004), Sheathfolds in rheomorphic ignimbrites, *Bull. Volcanol.*, *66*, 485–491.

Branney, M. J., B. Bonnichsen, G. D. M. Andrews, B. Ellis, T. L. Barry, and M. McCurry (2008), "Snake River (SR)-type" volcanism at the Yellowstone hotspot track: Distinctive products from unusual, high-temperature silicic super-eruptions, *Bull. Volcanol.*, *70*(3), 293–314.

Brumm, A., G. M. Jensen, G. D. van den Bergh, M. J. Morwood, I. Kurniawan, F. Aziz, and M. Storey (2010), Hominins on Flores, Indonesia, by one million years ago, *Nature*, *464*, 748–752, doi:10.1038/nature08844.

Bushnell, K. (1967), *Geology of the Rowland Quadrangle, Elko County, Nevada*, Mackay Sch. of Mines, Univ. of Nevada, Reno, Nev.

Cathey, H. E., and B. P. Nash (2004), The Cougar Point Tuff: Implications for thermochemical zonation and longevity of high-temperature, large-volume silicic magmas of the Miocene Yellowstone Hotspot, *J. Petrol.*, *45*, 27–58, doi:10.1093/petrology/egg081.

Coats, R. R. (1987), *Geology of Elko County, Nevada*, vol. 101, Nev. Bur. of Mines and Geol., Univ. of Nevada-Reno, Reno.

Coe, R. S., G. M. Stock, J. J. Lyons, B. Beitler, and G. J. Bowen (2005), Yellowstone hotspot volcanism in California? A paleomagnetic test of the Lovejoy flood basalt hypothesis, *Geology*, *33*(9), 697–700.

Dankers, P. H. M., and J. D. A. Zijderveld (1981), Alternating field demagnetization of rocks, and the problem of gyromagnetic remanence, *Earth Planet. Sci. Lett.*, *53*(1), 89–92.

Ellis, B. S., M. J. Branney, T. L. Barry, D. Barfod, I. Bindeman, J. A. Wolff, and B. Bonnichsen (2012), Geochemical correlation of three large-volume ignimbrites from the Yellowstone hotspot track, Idaho, USA, *Bull. Volcanol.*, *74*(1), 261–277.

Ellwood, B. B., J. C. Stormer, and J. A. Whitney (1989), Fish Canyon Tuff, Colorado: The problem of two magnetic polarities in a single tuff, *Phys. Earth Planet. Inter.*, *56*(3), 329–336.

Finn, D. R., and R. S. Coe (2016), A new protocol for three-axis static alternating field demagnetization of rocks, *Geochem. Geophys. Geosyst.*, *17*, 1815–1822, doi:10.1002/2015GC006178.

Finn, D. R., R. S. Coe, H. Kelly, M. Branney, T. Knott, and M. Reichow (2015), Magnetic anisotropy in rhyolitic ignimbrite, Snake River Plain: Implications for using remanent magnetism of volcanic rocks for correlation, paleomagnetic studies, and geological reconstructions, *J. Geophys. Res. Solid Earth*, *120*, 4014–4033, doi:10.1002/2014JB011868.

Fisher, R. A. (1953), Dispersion on a sphere, *R. Soc. London Proc. A*, *217*, 295–305.

Gattacceca, J., and P. Rochette (2002), Pseudopaleosecular variation due to remanence anisotropy in a pyroclastic flow succession, *Geophys. Res. Lett.*, *29*(8), 1286, doi:10.1029/2002GL014697.

Geissman, J. W., N. G. Newberry, and D. R. Peacor (1983), Discrete single-domain and pseudo-single-domain titanomagnetite particles in silicic glass of an ash-flow tuff, *Can. J. Earth Sci.*, *20*(2), 334–338.

Geissman, J. W., D. Holm, S. S. Harlan, and G. F. Embree (2010), Rapid, high-temperature formation of large-scale rheomorphic structures in the 2.06 Ma Huckleberry Ridge Tuff, Idaho, USA, *Geology*, *38*, 263–266, doi:10.1130/G30492.1.

Grommé, C. S., E. H. McKee, and M. C. Blake Jr. (1972), Paleomagnetic correlations and potassium argon dating of middle Tertiary ashflow sheets in the eastern Great Basin, Nevada and Utah, *Geol. Soc. Am. Bull.*, *83*(6), 1619–1638.

Hagstrum, J. T., and D. E. Champion (2002). A Holocene paleosecular variation record from ^{14}C-dated volcanic rocks in western North America. *J. Geophys. Res.*, *107*(B1), 2025, doi:10.1029/2001JB000524.

Hildreth, W., and G. A. Mahood (1985), Correlation of ash-flow tuffs, *Geol. Soc. Am. Bull.*, *96*, 968–974.

Jarboe, N. A., R. S. Coe, and J. M. Glen (2011), Evidence from lava flows for complex polarity transitions: The new composite Steens Mountain reversal record, *Geophys. J. Int.*, *186*(2), 580–602.

Jelinek, V. (1981), Characterization of the magnetic fabric of rocks, *Tectonophysics*, *79*(3-4), T63–T67.

Kirschvink, J. L. (1980), The least-squares line and plane and the analysis of palaeomagnetic data, *Geophys. J. Int.*, *62*(3), 699–718.

Knott, T. R., M. J. Branney, M. K. Reichow, D. R. Finn, R. S. Coe, M. Storey, D. Barford, and M. McCurry (2016a), Mid-Miocene record of large-scale Snake River-type explosive volcanism and associated subsidence on the Yellowstone hotspot track: The Cassia Formation of Idaho, USA, *Geol. Soc. Am. Bull.*, doi:10.1130/B31324.1.

Knott, T. R., M. K. Reichow, M. J. Branney, D. R. Finn, R. S. Coe, M. Storey, and B. Bonnichsen (2016b), Rheomorphic ignimbrites of the Rogerson Formation, central Snake River Plain, USA: Record of mid-Miocene rhyolitic explosive eruptions and associated crustal subsidence along the Yellowstone hotspot track, *Bull. Volcanol.*, *78*(4), 1–25.

Lee, J. Y., K. Marti, J. P. Severinghaus, K. Kawamura, H. S. Yoo, J. B. Lee, and J. S. Kim (2006), A redetermination of the isotopic abundances of atmospheric Ar, *Geochim. Cosmochim. Acta*, *70*, 4507–4512, doi:10.1016/j.gca.2006.06.1563.

Manley, C. R., and W. C. McIntosh (2002), The Juniper Mountain volcanic center, Owyhee County, southwestern Idaho: Age relations and physical volcanology. Tectonic and magmatic evolution of the Snake River plain volcanic province, *Idaho Geol. Surv. Bull.*, *30*, 205–227.

Min, K., R. Mundil, P. R. Renne, and K. R. Ludwig (2000), A test for systematic errors in ^{40}Ar/^{39}Ar geochronology through comparison with U/Pb analysis of a 1.1-Ga rhyolite, *Geochim. Cosmochim. Acta*, *64*, 73–98, doi:10.1016/S0016-7037(99)00204-5.

Morgan, L. A., and W. C. McIntosh (2005), Timing and development of the Heise volcanic field, Snake River Plain, Idaho, western USA, *Geol. Soc. Am. Bull.*, *117*(3-4), 288–306.

Morris, E. R., W. Schillinger, R. S. Coe, C. J. Pluhar, and N. A. Jarboe (2009), Automating the 2G superconducting rock magnetometer for single-solenoid alternating field demagnetization, *Geochem. Geophys. Geosyst.*, *10*, Q05Y05, doi:10.1029/2008GC002289.

Ort, M. H., S. L. de Silva, N. C. Jiménez, B. R. Jicha, and B. S. Singer (2013), Correlation of ignimbrites using characteristic remanent magnetization and anisotropy of magnetic susceptibility, central Andes, Bolivia, *Geochem. Geophys. Geosyst.*, *14*, 141–157, doi:10.1029/2012GC004276.

Perkins, M. E., W. P. Nash, F. H. Brown, and R. J. Fleck (1995), Fallout tuffs of Trapper Creek, Idaho—A record of Miocene explosive volcanism in the Snake River Plain volcanic province, *Geol. Soc. Am. Bull.*, *107*(12), 1484–1506.

Pierce, K. L., and L. A. Morgan (1992), The track of the Yellowstone hot spot: Volcanism, faulting, and uplift, *Geol. Soc. Am. Mem.*, *179*, 1–54.

Pioli, L., R. Lanza, M. Ort, and M. Rosi (2008), Magnetic fabric, welding texture and strain fabric in the Nuraxi Tuff, Sardinia, Italy, *Bull. Volcanol.*, *70*(9), 1123–1137.

Pouchou, J. L., and F. Pichoir (1985), "PAP" procedure for improved quantitative analysis, *Microbeam Anal.*, *20*, 104–105.

Powell, R., J. Hergt, and J. Woodhead (2002), Improving isochron calculations with robust statistics and the bootstrap, *Chem. Geol.*, *185*, 191–204, doi:10.1016/S0009-2541(01)00403-X.

Reynolds, R. L. (1977), Paleomagnetism of the welded tuffs of the Yellowstone group, *J. Geophys. Res.*, *82*, 3677–3693, doi:10.1029/JB082i026p03677.

Rivera, T. A., M. Storey, C. Zeeden, F. J. Hilgen, and K. Kuiper (2011), A refined astronomically calibrated ^{40}Ar/^{39}Ar age for Fish Canyon sanidine, *Earth Planet. Sci. Lett.*, *311*(3), 420–426.

Rosenbaum, J. G. (1986), Paleomagnetic directional dispersion produced by plastic deformation in a thick Miocene welded tuff, southern Nevada: Implications for welding temperatures, *J. Geophys. Res.*, *91*, 12,817–12,834, doi:10.1029/JB091iB12p12817.

Sagnotti, L. (2013), Demagnetization Analysis in Excel (DAIE). An open source workbook in Excel for viewing and analyzing demagnetization data from paleomagnetic discrete samples and u-channels, *Ann. Geophys.*, *56*(1, D0114).

Schlinger, C. M., J. G. Rosenbaum, and D. R. Veblen (1988), Fe-oxide microcrystals in welded tuff from southern Nevada: Origin of remanence carriers by precipitation in volcanic glass, *Geology*, *16*(6), 556–559.

Sharp, R. P. (1939), The Miocene Humboldt Formation in northeastern Nevada, *J. Geol.*, 133–160.
Speranza, F., A. Di Chiara, and S. G. Rotolo (2012), Correlation of welded ignimbrites on Pantelleria (Strait of Sicily) using paleomagnetism, *Bull. Volcanol.*, *74*, 341–357, doi:10.1007/s00445-011-0521-9.
Stephenson, A., S. Sadikun, and D. K. Potter (1986), A theoretical and experimental comparison of the anisotropies of magnetic susceptibility and remanence in rocks and minerals, *Geophys. J. Int.*, *84*(1), 185–200.
Wolff, J. A., B. B. Ellwood, and S. D. Sachs (1989), Anisotropy of magnetic susceptibility in welded tuffs: Application to a welded-tuff dyke in the Tertiary Trans-Pecos Texas volcanic province, USA, *Bull. Volcanol.*, *51*(4), 299–310.